Quantify and account for field reference errors in forest remote sensing studies

Henrik Jan Persson [a,*], Magnus Ekström [a,b], Göran Ståhl [a]

[a] *Department of Forest Resource Management, Swedish University of Agricultural Sciences (SLU),Umeå, Sweden*
[b] *Department of Statistics, USBE, Umeå University, Umeå, Sweden*

ARTICLE INFO

ABSTRACT

Field inventoried data are often used as references (ground truth) in forest remote sensing studies. However, the reference values are affected by various kinds of errors, which tend to make the reported accuracies of the remote sensing-based predictions worse than they are. The more accurate the remote sensing techniques are becoming, the more pronounced this problem will be. This paper addresses the impact of uncertainties in field reference data due to measurement errors, model errors, and position errors when evaluating the accuracy of biomass predictions from airborne laser scanning at plot level. We present novel theoretical analysis methods that take the interactions of the error sources into account. Further, an error characterization model (ECM) is used to describe the error structure of the remote sensing-based predictions, and we show how the parameters of the ECM can be adjusted when field references contain errors. We also show how root mean square error (RMSE) estimates can be adjusted. Based on data from Scandinavian forests, we conclude that the field reference errors have an impact on the remote sensing-based predictions. By accounting for these errors the RMSE of the remote sensing-based predictions was reduced by 6–18%. The most influential sources of error in the field references were found to be the residual errors of the allometric biomass model and the field plot position errors. Together, these two sources accounted for 97% of the variance while measurement errors and biomass model parameter uncertainties were negligible in our study.

1. Introduction

Remote sensing (RS) is used in many forest applications, often in combination with field sample plots to enable wall-to-wall assessment of some variable of interest (VOI) across a study area. This type of survey, communicated as maps or predictions of means and totals, is becoming increasingly demanded, not least in connection with assessing carbon budgets for forests where the VOI typically is biomass (Rodríguez-Veiga et al., 2019). A challenge in this type of studies is to correctly assess uncertainties (Gregoire et al., 2016).

Broadly speaking, the uncertainty assessment in RS studies proceeds along either of two very different lines. The first category use RS data as auxiliary data in formal statistical procedures for estimating means or totals of the VOI across the study area. Typical approaches include model-assisted estimation within the framework of design-based inference (Ekström and Nilsson, 2021; McRoberts et al., 2014a, 2016; Ståhl et al., 2016; Stehman, 2009) and model-based inference (McRoberts, 2006; McRoberts et al., 2007, 2010, 2016; Ståhl et al., 2011). In this case, strict statistical principles for the selected inferential mode should be followed (Gregoire et al., 2016). Typically, the variance or the mean square error of the estimated VOI is estimated and reported, often in the form of a confidence interval for the true VOI value (McRoberts et al., 2010, 2014b, 2016).

The other category of approaches addresses the uncertainty assessment in a more intuitive way, often in connection with studies aiming at assessing the performance of some new RS method or technique. A typical procedure in this type of studies includes the following steps: (1) inventory a number of field sample plots for the VOI, (2) extract the corresponding plot-level RS data, (3) fit a model that relates the RS data to the field sample data, (4) apply the model to the entire RS dataset, and (5) quantify the uncertainty of predictions at plot or stand level through paired reference unit comparisons (PRUC) of the RS-based predictions and the field references on validation data (Mauya et al., 2015; Næsset, 2004a; Næsset and Gobakken, 2008; Persson and Fransson, 2014, 2017; Tomppo et al., 2008; Varvia, 2018). This may be repeated for different sensors, methods, regions or sensor properties, in order to assess

---

* Corresponding author.
  E-mail address: Henrik.Persson@slu.se (H.J. Persson).

strengths and limitations of one or more RS-based methods of interest. The uncertainty following the PRUC approach is often reported as the empirical mean square error (or root mean square error, RMSE) at the level of assessment units (typically plots or stands), treating field inventoried data as true values. The dataset is sometimes separated into a training and an evaluation part, or cross-validation is applied in order to utilize the full dataset for model training (Stone, 1974). It is important to note that uncertainty assessment following the second approach is quite different from uncertainty assessment following the first approach and that different questions are answered (Persson and Ståhl, 2020; Ploton et al., 2020). The core objective using the first category is to provide confidence intervals for the mean or total of the VOI for the entire study area. The core of the second approach (PRUC) is to report the uncertainty of a certain RS method at the level of a typical assessment unit, such as a plot or a stand. When the PRUC approach is adopted, the results can usually not be extrapolated to valid uncertainty inferences for the entire study area (cf. Gregoire et al., 2016).

In this paper, we address the uncertainty assessment for the PRUC approach. It involves several challenges that do not occur in a similar way for the first category. One such challenge is that the development of RS has enabled RS-based predictions to be so accurate that any potential, often minor, errors in the field references cannot be neglected, since if they were, they would inflate the reported accuracies of the RS-based predictions. In the past this complication could be neglected, since any errors in the field references were vastly surpassed by those in the RS-based predictions. However, today there is an increasing need of quantifying and correcting for such field reference-related errors. In Persson and Ståhl (2020), four dominant error sources were identified: sampling errors, measurement errors, model errors, and plot position errors, although only the effect of sampling errors was addressed in that case study. It was suggested that a linear error characterization model (ECM) could be used as a means for more sophistically describing uncertainties of RS-based predictions compared to using simpler metrics, such as the RMSE, and it was demonstrated how the parameter estimates of the ECM could be corrected for the impact of (random) errors in the field references, which caused attenuation bias of the parameter estimates. This was shown to be particularly important when the errors in RS-based predictions tended to be as small as those in the field references. The quantification of the impact of sampling errors in the field references has been repeated for other studies and datasets (de Lera Garrido et al., 2020; Persson et al., 2020, 2021), where the sampling errors have had a significant impact on the reported accuracies. Often it is also the largest error source in case of the first category of uncertainty assessment (Gertner and Köhl, 1992). Similarly, it was noted that ignoring an informative sampling design may yield severely biased estimates of regression coefficients (Ekström et al., 2018).

When the purpose of a field inventory is to assess the accuracy of RS-based predictions through PRUC at the level of plots, there is no sampling error involved (since all trees in the plots are inventoried) and the other, normally small, error sources become increasingly important (Gertner and Köhl, 1992). The measurement errors in field inventories following strict protocols are typically relatively small (Broman and Christoffersson, 1999; Fridman et al., 2019) and it can be assumed that their contribution to the total error is limited. However, if there is no sampling error involved the relative magnitude of measurement errors in comparison to other errors may be considerable and thus we chose to include them in this study. The use of a model is required when the target variable cannot be directly measured, but must be predicted from other measured variables. A typical example is aboveground biomass (AGB) which may be modelled from the tree diameter and height. Parresol (1999) addressed many of the challenges and questions involved in this type of modeling in an extensive review of assessing tree and stand biomass. Assuming a correct model is specified (Berry and Feldman, 1985), the model uncertainty may be divided into (i) uncertainty due to model parameters being estimated and (ii) uncertainty due to random variation at the level of individual units (residual errors). When a model

is applied across a large region for predicting means or totals, the first kind of uncertainty tends to be the most influential one whereas for smaller areas the second category tends to be most important (Berger et al., 2014; Breidenbach et al., 2014; Ståhl et al., 2016; Wharton and Cunia, 1987). However, other factors may need to be considered as well in the context of handling model errors. Gregoire et al. (1995) investigated within-plot correlated tree-level errors using mixed-effect models and stressed the importance of considering this type of correlation, which may greatly affect the results in some types of studies. Meng and Huang (2010) investigated this aspect from the perspective of growth and change using longitudinal data, and reached a similar conclusion. Fox et al. (2001) found that studies that ignore the correlation within plots underestimate the variability between plots, as well as the variance of the model parameter estimators.

When sample plots are used in a design-based approach to estimate the total or mean for a study area, the precision of plot locations is of minor importance, provided the plots are randomly located within the study area. However, when sample plots are coupled with external geographical data, such as RS data, the effects of position errors must be considered (Coulston et al., 2004; DeCesare et al., 2005; Frazer et al., 2011; Hernández-Stefanoni et al., 2018; McRoberts et al., 2018; Saarela et al., 2016; Sigrist et al., 1999). The plot locations are normally measured using a global navigation satellite system (GNSS), e.g., the global positioning system (GPS). When the field position error is small in proportion to the pixel size of the RS source, position errors can usually be ignored, but otherwise their impact can be substantial (Weber, 2006; Weber et al., 2008). The position errors (GNSS inaccuracies) have a random behavior that is affected by stand conditions and the GNSS accuracy is lower when the GNSS is shadowed by dense forest canopy (Frair et al., 2010; Valbuena et al., 2010). Typical forest plot location errors reported in the literature range from about 1 m when using a dGPS or real-time kinematic (RTK) GPS, to about 5 m or more for standard handheld devices (Berglund, 2000; Friberg and Jönsson, 2012; Galán et al., 2011; Johansson, 2019; McRoberts et al., 2018; Piedallu and Gégout, 2005; Saarela et al., 2016; Valbuena et al., 2010). Experience from field inventory personnel and informal tests from different groups indicate that the errors tend to increase with increasing basal area and canopy closure due to increasing scattering within the canopy. Formal studies have confirmed this with respect to forest density (Næsset and Gjevestad, 2008) and degree of canopy closure (Frair et al., 2010). The consequence of using incorrect plot center coordinates (or inaccurately positioned RS data) is that neighboring trees are measured instead of the intended (or correspondingly, that the nearby pixels are used instead). When inventory data are available from the neighborhood of the field sample plots, it is possible to assess the accuracy of plot-level AGB estimates due to GNSS uncertainty using Monte Carlo simulations (McRoberts et al., 2005; Saarela et al., 2016). By perturbing the plot center coordinates for the plot, other trees will be included in the plot measurements and hence contribute to the predicted AGB.

In the current paper, we extend the study by Persson and Ståhl (2020), which addressed how the parameters of an ECM could be corrected in the presence of sampling errors in stand-level field references. In the current study we focus on plot-level assessments and investigate the impact of measurement errors, model errors, and plot position errors in the field references, for the case when the uncertainty assessment of RS-based predictions is made through PRUC.

The specific objectives of the study were to:

1. Describe the generic impact of how measurement errors, model errors, and plot position errors in the field references affect the apparent accuracy of RS-based predictions.
2. Develop and evaluate methods to correct for field reference errors.
3. Quantify the impact of different error sources and hence identify which error sources are most critical to address for correctly reporting the uncertainty of RS-based predictions.

2. Data

2.1. Study area

Two study areas were used for the four case studies and, additionally, field data distributed across Sweden (Fig. 1 a) were used for developing national biomass models. The first study area was the Krycklan (Fig. 1 b) river catchment, located in northern Sweden (Lat. 64°16′N, Long. 19°46′E), comprising 7470 ha land. The main tree species are Scots pine (*Pinus sylvestris* L.), mainly in dry upslope areas, Norway spruce (*Picea abies* (L.) H.Karst), mainly in wetter lowland areas, and birch (*Betula pendula* and *Betula pubescens*) in riparian forests along larger streams. The region is hilly with elevations ranging between 125 and 350 m above sea level. The second study area was the Remningstorp estate (Fig. 1 c), located in southern Sweden (Lat. (58°30′N, Long. 13°40′E), comprising 1300 ha. The forest is dominated by Norway spruce (*Picea abies* (L.) H.Karst.) and Scots pine (*Pinus sylvestris* L.) with some birch (*Betula* spp.). The region is rather flat with elevations ranging between 120 and 145 m above sea level.

2.2. Field data

Data from two independent inventories were used in each of the study areas. The first inventory consisted of 28 (Krycklan, Fig. 1 b) and 40 (Remningstorp, Fig. 1 c) circular plots with 40 m radius, performed in 2015 and 2014, respectively. The locations of the plots were subjectively selected to approximately represent the different forest conditions within the study areas, in terms of biomass range, tree species, and age structure. Each plot was entirely enclosed by its management unit, hence representing quasi-homogenous forest. Every tree was positioned using a differential GPS (dGPS). The second inventory at each study area consisted of a systematic grid with random starting position, providing 351 plots in Krycklan and 219 plots in Remningstorp, respectively. These 10 m radius plots were inventoried in the fall 2015 and 2014, respectively.

The distribution of plots within the test sites is shown in Figs. 1 b and c. The plot locations were measured using a Trimble GeoExplorer 6000 GeoXR (assumed to provide an accuracy of 1 m), and all trees with a diameter at breast height (DBH) ≥ 0.04 m were calipered. The height was measured on a sub-sample of the trees, using a hypsometer. The AGB was estimated for each tree using existing allometric models with tree species and DBH as explanatory variables, and the trees were then aggregated to plot-level values (Marklund, 1988).

To assess AGB model uncertainty, we used the original dataset from Marklund (1988). It contains the trees that were used to estimate model parameters for modeling the biomass (by fractions) of pine, spruce and birch trees in Sweden. In our case, AGB included all biomass fractions above the stump. These models have been extensively used and cited, and these models are still used for estimating and reporting national forest carbon stocks and changes. The trees were collected from 131 stands distributed across Sweden, providing a good representation of various stand ages and site conditions (Fig. 1 a). In total, 1286 trees from 490 plots within the stands were felled and the weight of the dry biomass fractions were measured for 493 pines, 551 spruces, and 242 birches. We identified 13 trees that were removed, due to missing plot coordinates or being outliers. Details are available in the original reference.

2.3. RS data

Airborne-laser-scanning (ALS) data were acquired from the Krycklan study area on 22 and 23 August 2015 with a Titan L359 laser scanner at 300 kHz PRF, providing >20 points/m² density. The wavelength was
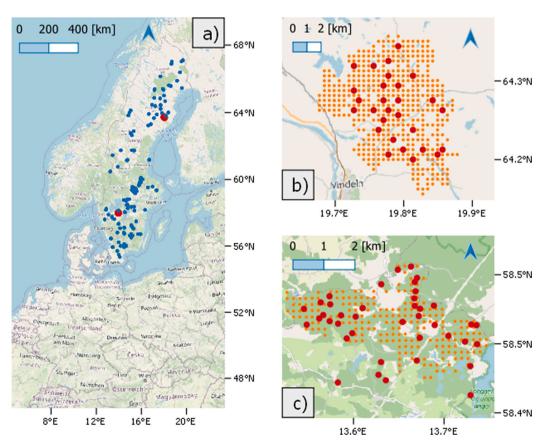

Fig. 1. a) Overview of Sweden with the plot locations in dark blue marking sample tree locations used for estimating the AGB models. The locations of the test sites are marked in red. Coordinates in Lat-Lon, EPSG4326. b) The northern test area Krycklan and c) the southern test area Remningstorp, in both sites with the 10 m field plots in orange and the 40 m plots in red. (For interpretation of the references to colour in this figure legend, the reader is referred to the web version of this article.)

1064 nm. The Remningstorp estate was scanned on 4 August 2014 with a Riegl LMS 680i laser scanner at 240 kHz PRF, providing >20 points/m^2. The wavelength was 1550 nm.

3. Methods

In this section we first address the generic impact of the different error components (see Table 1 for an overview of some notations). Second, we repeat the main results from Persson and Ståhl (2020) to describe what quantitative information about the error sources are needed for adjusting the parameters of an ECM or for adjusting an RMSE estimate that includes field reference errors. Third, we present a novel analysis approach for quantifying field reference uncertainty due to errors arising from measurements, modeling, and positioning of plots, taking into account interactions between the error sources. Lastly, we describe the case studies and put all parts together.

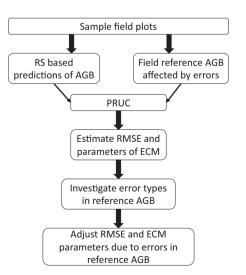The approach presented in the current manuscript is summarized in Fig. 2.

3.1. Error sources

The theory presented in this paper is developed for non-categorical target variables, and we demonstrate it for AGB, evaluated at the plot level. We assume that a number of sample plots have been selected from

Table 1
Most important notations in the manuscript (not complete list).

Notation	Explanation
T_{RS}	RS based prediction (e.g., of a single tree AGB).
T	True value, which in practice can never be observed.
λ_0, λ_1	ECM intercept and slope parameters.
ε	Residual error in RS model of the true value (random error).
σ_X	Standard deviation of variable X.
α	Parameter in the remote sensing model of AGB.
β	Parameter in the field model of AGB.
$*$	Indicates a corrected value (e.g., for attenuation bias).
x_{jkl}	Explanatory field variable l for tree j on plot k (to estimate field AGB). Lowercase to stress it is not random.
η_{jkl}	Measurement error of the variable x_{jkl}.
$\widetilde{X}_{jk}$	Explanatory variable including measurement error ($\widetilde{X}_{jkl} = x_{jkl} + \eta_{jkl}$). The uppercase notation indicates it is random due to the random measurement errors and bold is used for denoting vectors.
f, g	Functions to describe the relation between response variable and explanatory variables.

Fig. 2. Flowchart illustrating the method structure. The emphasis of this paper is on the two lowest boxes – investigate and apply adjustments.

the study area. For each plot we have access to tree-level measurements of diameter, height, etc. that allow us to use existing models for estimating the AGB for each tree (Marklund, 1987), which are aggregated to plot-level values normalized with the plot area, and expressed as tons per hectare. The model for estimation of AGB is normally nonlinear in relation to the measured tree attributes (Jucker et al., 2017). We also have access to plot averages of RS data extracted for areas that correspond to the plots. Each plot center has a GNSS coordinate. The plots may be randomly or non-randomly selected from the study area, and they may purposively have been selected from some type of forest of particular interest for the investigation.

The plots are divided into two groups: one group is used for estimating models linking field and RS data. The other group of plots is used for evaluating the uncertainties of the model predictions. Similar to Persson and Ståhl (2020) we quantify uncertainties through, (i) an ECM, and (ii) computing RMSE.

Three error sources are addressed:

- Measurement errors, i.e., errors conducted during the fieldwork causing measured diameters etc. for the trees to deviate from the true ones. Several studies have quantified random errors related to measuring trees (Gertner, 1986, 1987; Kendall et al., 1987), while the systematic errors (biases) normally tend to be small. Trees on plots may also be entirely missed or double counted. In our study the magnitude of measurement errors were retrieved from the control surveys of plots conducted in the Swedish National Forest Inventory (Fridman et al., 2014, 2019). When calipered tree diameters are used in models, the measurement errors propagate, i.e., their magnitude may be inflated through the model and even if the measurement errors are only random, a non-linear AGB model might make the predictor of AGB biased (Suty et al., 2013).
- Model errors of different kinds. The main types of model errors include model specification errors (Berry and Feldman, 1985), parameter estimation errors (Beck and Arnold, 1977), and model residual errors (Buonaccorsi, 2010; Fuller, 1987). Two main models are involved in the assessment procedure: the model used for estimating plot-level characteristics from the basic tree-level measurements (AGB from tree diameter), and the model linking RS data with field reference data. We are interested in evaluating the performance of the second model (using the error model introduced in the next section), but in doing so uncertainties linked to the first model affect our evaluation. Therefore, we address parameter estimation errors and residual errors of the first model, but we assume that the model is correctly specified.
- Plot position errors. Depending on what type of georeferencing equipment is used, the magnitude of position errors will differ. Various measures are used to report the accuracy, including circular error probability, distance root mean square error (DRMS), and radius 95 (R95) (Chin, 1987; Devon et al., 2015; NovAtel, 2003). We use DRMS and provide a definition in section 3.4.1, but regardless of measure their order of magnitude correspond. In our studies we addressed the effects of this type of errors, and their potential interactions with other errors through simulations based on inventory data from a larger surrounding than the 10 m plots, where all trees had been calipered and positioned with a real-time kinematic (RTK) GPS.

All three sources of errors may decrease the apparent accuracy of RS-based predictions of AGB. The challenge is to understand the impact of, and potentially adjust for, the errors when estimating the RMSE or the parameters of the ECM.

3.2. Error characterization model (ECM)

To characterize errors in RS-based estimates, a linear ECM was introduced in Persson and Ståhl (2020), following Tian et al. (2016). In

this study we use it at the plot level. The ECM is expressed as a simple linear model,

$$T_{RS} = \lambda_0 + \lambda_1 T + \varepsilon, \tag{1}$$

where T_{RS} denotes the predicted value based on RS data, T the true value, λ_0 a systematic displacement which remains the same across the entire range of true values, and λ_1 a parameter that shows how the systematic error changes across the range of true values. The dispersion of the random error terms, ε, is quantified with the standard deviation, σ_ε. Thus, if true field observations are available, we can regress T_{RS} on T to obtain unbiased estimates of the above parameters (Buonaccorsi, 2010; Carroll et al., 2006; Fonseca et al., 2005; Wilks, 2011). In contrast to reporting a single RMSE value (Hyyppä et al., 2000; Næsset, 2004b; Nilsson, 1997; Persson et al., 2017; Persson and Fransson, 2017), presenting the parameter estimates from the ECM offers additional insights about the error structure of the RS-based estimates. Also, the ECM facilitates comparisons with other studies, since the errors for specific reference values can be estimated and compared.

However, with errors in the field references, we observe T_{ref} instead of the true value T. If the errors are random they will cause attenuation bias in the estimated ECM parameters (bias toward 0 in the model coefficients caused by measurement errors in the explanatory variables). Estimators that correct for this were provided in Persson and Ståhl (2020), and are repeated here for clarity.

The intercept of the ECM is denoted by λ_0, the slope of the ECM by λ_1, and σ_ε is the standard deviation of the random error for a given reference value.

$$\widehat{\lambda}_1^* = \widehat{\lambda}_1 \left[1 + \frac{\widehat{\sigma}_R^2}{\widehat{\sigma}_{T_{Ref}}^2 - \widehat{\sigma}_R^2} \right], \tag{2}$$

$$\widehat{\lambda}_0^* = \overline{T}_{RS} - \widehat{\lambda}_1^* \overline{T}_{Ref}, \tag{3}$$

$$\widehat{\sigma}_\varepsilon^{2*} = \widehat{\sigma}_\varepsilon^2 \frac{\left[1 - \frac{r^2 \bullet \widehat{\sigma}_{T_{Ref}}^2}{\widehat{\sigma}_{T_{Ref}}^2 - \widehat{\sigma}_R^2} \right]}{1 - r^2}. \tag{4}$$

The * notation is used to denote a corrected value, $\overline{\bullet}$ mean values, $\widehat{\bullet}$ estimated values, $\widehat{\sigma}_\varepsilon^2$ denotes the residual variance from regressing T_{RS} on T_{Ref}, r is the sample Pearson correlation coefficient between T_{RS} and T_{Ref}, and $\widehat{\sigma}_{T_{Ref}}^2$ is the estimated empirical variance among the field reference values, i.e., the available field reference values are used in a sample variance formula.

The term $\widehat{\sigma}_R^2$ is at the core of our analysis, since it is key to adjusting the ECM with regard to errors in the field references. It is the estimated variance of the random errors in the field references, i.e., in our case the combined effect of measurement, modeling, and position errors. In the case studies, we assume this variance to be homogeneous across the range of studied true values. However, simulations have indicated robust results of the ECM also when this assumption is not met. A major part of the remainder of this paper is devoted to assessing the magnitude of σ_R^2 based on empirical data. As will be seen, our methods also allow for the estimation of potential systematic errors in T_{Ref}, although in PRUC-based assessments some systematic errors will have the same magnitude in the data used for model estimation and model evaluation and thus will not be detected. This issue will be further covered in the discussion. To apply the proposed methods we need to show that the magnitude of systematic errors in T_{Ref} is small and we need to quantify σ_R^2 based on existing data, and apply the estimate in formulas (2)–(4).

In Persson and Ståhl (2020), we used the formulas (2)–(4) with case study data at stand level where sampling errors were assumed to be the dominating source of the random errors. In this study, the random errors are instead assumed to constitute the sum of plot level random errors due to measurement errors, model errors, and position errors. The

estimated variance of their sum is the sum of their respective estimated variances plus any covariances, as will be shown in the next section.

In case our interest is the MSE (or RMSE) rather than the parameters of the ECM, we can make adjustments in a similar way by taking the sum of the squared bias and the squared corrected standard deviation (5):

$$\widehat{MSE}^* = \left(\overline{T}_{RS} - \overline{T}_{Ref} \right)^2 + \widehat{\sigma}_\varepsilon^{2*}. \tag{5}$$

Through such a correction, we are able to assess the actual reliability of the RS-based predictions rather than the apparent reliability, distorted by measurement, modeling and position errors in the field references.

3.3. Impact of and interaction between error sources

To develop a strict definition of the interactions between the error sources and to find a way of estimating their impact on RS-based predictions, we assume that a forest is inventoried in the field by measuring single trees on circular plots with a fixed radius. The tree attributes are denoted x_{jkl}, where j is an index for the trees, k for the plots, and l is an index for the measured variables (e.g., DBH, height, species etc.). During the field survey, measurement errors denoted η_{jkl} are committed, i.e., we measure $\widetilde{X}_{jkl} = x_{jkl} + \eta_{jkl}$, which thus includes the random measurement error. In vector notation (with the vector elements being the measured variables), we may write $\widetilde{X}_{jk} = x_{jk} + \eta_{jk}$. Some variables of interest cannot (easily) be measured directly (e.g., VOL and AGB), and are hence predicted using some function $f(x_{jk}, \beta)$ with attribute-vector x_{jk} and parameter-vector β.

In environmental research, the relations are often non-linear with respect to the variable of interest. For example, the function may take a log-transformed form of the response variable, as in our case study where it was log(AGB) instead of AGB for the biomass of a tree, to enable a linear form of the regression model. The back-transformed model then takes an exponential form.

Let $T_{jk} = \exp(f(x_{jk}, \beta) + \varepsilon_{jk}) = \exp(f(x_{jk}, \beta)) \exp(\varepsilon_{jk})$ denote the true AGB of tree j in plot k, where ε_{jk} is a random residual error. If logarithms are taken on both sides we obtain $log(T_{jk}) = f(x_{jk}, \beta) + \varepsilon_{jk}$, which can be regarded as a regression model with a log-transformed response variable. In addition, we can express the true AGB for a plot k as

$$T_k = \sum_{j \in M_k} exp(f(x_{jk}, \beta) + \varepsilon_{jk}) = \sum_{j \in M_k} exp(f(x_{jk}, \beta)) exp(\varepsilon_{jk}), \tag{6}$$

where M_k denotes all trees on plot k, positioned without errors. The true AGB of tree j on plot k is estimated using $exp\left(f\left(\widetilde{X}_{jk}, \widehat{\beta}\right)\right) exp(s_{jk})$, where s_{jk} denotes a correction for logarithmic bias and where $exp(s_{jk}) = E(exp(\varepsilon_{jk}))$, or at least fulfills that $exp(s_{jk})$ is a good approximation of E $(exp(\varepsilon_{jk}))$ (Clifford et al., 2013; Smith, 1993).

Next, we introduce plot position uncertainty, $\rho_k = (\rho_{k1}, \rho_{k2})^T$, where T denotes the transpose, which describes the error of the plot center in northing and easting, respectively. The position error causes us to measure the trees j in M_k' instead of in M_k, where M_k' denotes the trees on an incorrectly positioned plot. Then, the observed plot AGB is

$$T_{ref,k} = \sum_{j \in M_k'} exp\left(f\left(\widetilde{X}_{jk}, \widehat{\beta}\right)\right) exp(s_{jk}). \tag{7}$$

To simplify the notation, let $g(x_{jk}, \beta) = \exp(f(x_{jk}, \beta))$. A first-order Taylor approximation of the nonlinear function g can be used to derive three error terms R_1, R_2, and R_3, related to the errors we address in this paper, and their corresponding expectations, variances, and covariances (Lee and Forthofer, 2006). Their definitions are described in the following sections, and the complete derivation is presented in Appendix A1. The derivation leads to three error components, related to four dominating error sources. By using Taylor approximation we can

express the difference between the measured and true biomass on a plot as:

$$T_{ref,k} - T_k \approx R_{1k} + R_{2k} + R_{3k}, \tag{8}$$

where

$$R_{1k} = \sum_{j \in M'_k} exp(s_{jk}) \sum_{l=1}^{p} \eta_{jkl} \frac{\partial g(\boldsymbol{x}_{jk}, \boldsymbol{\beta})}{\partial x_{jkl}} \tag{9}$$

is a contribution originating from the measurement errors (errors in the explanatory variables) and position error (which causes us to include the trees M'_k on the inaccurate plot position, $T_{ref,k}$, instead of the trees M_k on the true plot position, T_k). Control inventories (which we use in this paper) can be used in practice to estimate the expected value of R_{1k} and its variance.

Then, we consider

$$R_{2k} = \sum_{j \in M'_k} exp(s_{jk}) \sum_{i=0}^{p} (\widehat{\beta}_i - \beta_i) \frac{\partial g(\boldsymbol{x}_{jk}, \boldsymbol{\beta})}{\partial \beta_i} \tag{10}$$

as the error contribution originating from parameter estimation uncertainties (applied to trees on the incorrectly positioned plot), since a sample was used to estimate the parameters. Increasing the sample size would decrease the uncertainty about the parameter estimates and additional samples would be necessary to estimate the expected value of R_{2k}. However, the procedure of collecting a sample for developing biomass models is tedious and time consuming and, hence, usually limits the sample size due to the costs involved. As we will see, the impact of this error component is small and in practice, both training and evaluation trees are affected in the same way in case of incorrect parameter values (given that training and evaluation data are distributed similarly). In this study, we use the Taylor approximation of the biomass models together with the covariance matrices for the estimated model parameters from the biomass models to estimate this component for single trees, and through simulations we explored the impact of inaccurate plot positions and how this component may vary with reference biomass.

Finally,

$\delta_k + \tau_{jk}$, corresponding to a random error δ_k specific to plot k, and an error term τ_{jk} for tree j on plot k. This form was chosen after a variance component analysis based on Marklund's original data, covering entire Sweden. Even at fairly small geographical scales, the analysis did not indicate any correlated residuals between plots. However, within plots there was an effect which agreed with previous studies that have shown that tree-level residuals tend to be correlated at this scale (Breidenbach et al., 2014; Lehtonen et al., 2007; Repola, 2009).

For a given position error ρ_k, conditional expectations and variances of the errors R_{1k} and R_{2k} were derived in a similar way as in Gertner (1987, 1990) and these were needed to derive corresponding unconditional expectations and variances. The analogous derivations for R_{3k} were a bit more tedious (see Appendix A1 for details). Subsequently, unconditional expectations and variances for R_{1k}, R_{2k}, and R_{3k} were obtained through the law of total expectation and the law of total variance, respectively. In cases where analytical expressions were too complex to be solved, Monte Carlo simulations were used. These simulations were used only when taking position errors into account.

The obtained unconditional expectations and variances are valid for plots with a single tree species. When plots contain combinations of trees of different species, the variance expressions get increasingly complex (see Appendix A1), with additional covariance terms. The implementation in our case study considered three tree species. The Monte Carlo simulations allowed us to estimate both the biases (systematic errors) and the variances for each of the error components (R_1, R_2, and R_3).

3.4. Empirical case study

To quantify the impact of the field reference errors, we applied the developed theory (and Monte Carlo simulations) to real data in the two case study areas: Krycklan and Remningstorp (see section 2.1). The assumptions related to the simulations are presented in section 3.4.1. To assess the overall influence of the field reference errors in remote sensing studies, we demonstrated the implications in four case studies (A-D) across the two study areas. These enabled us to demonstrate the overall framework, as well as the impact of different assumptions, under different forest conditions and remote sensing datasets. In each test site, we used the same ALS remote sensing data, but combined with two

$$R_{3k} = \sum_{j \in M'_k \cap M_k} g(\boldsymbol{x}_{jk}, \boldsymbol{\beta}) \left(exp(s_{jk}) - exp(\varepsilon_{jk}) \right) + \left\{ \sum_{j \in M'_k \setminus M_k} g(\boldsymbol{x}_{jk}, \boldsymbol{\beta}) exp(s_{jk}) - \sum_{j \in M_k \setminus M'_k} g(\boldsymbol{x}_{jk}, \boldsymbol{\beta}) exp(\varepsilon_{jk}) \right\} \tag{11}$$

contains both errors related to the position errors of the plots and the residual errors of the AGB model. The set operator $M'_k M_k$ denotes all trees in M'_k that are not included in M_k, and $M_k \setminus M'_k$ the opposite. This is the error component most affected by the incorrectly positioned plot locations. Therefore, to estimate the expectation and variance of R_{3k}, we need the single trees to be measured both on the correctly and incorrectly positioned plots, and the residual errors from the biomass functions.

To single out the impact of the position error (which is twinned with the other errors, e.g., the residual error in R_{3k}), we can perform the analysis with and without position error and study the difference. Without the position error, R_1 and R_2 can be derived using summation over M_k (instead of M'_k). Similarly, the two last components in R_3 will be zero ($\sum_{j \in M'_k \setminus M_k} g(\boldsymbol{x}_{jk}, \boldsymbol{\beta}) exp(s_{jk})$ and $\sum_{j \in M_k \setminus M'_k} g(\boldsymbol{x}_{jk}, \boldsymbol{\beta}) exp(\varepsilon_{jk})$).

The residual errors of trees within plots are correlated and to handle this, we assume that the residual random error can be expressed as $\varepsilon_{jk} = $

different field reference datasets. First, one smaller dataset (case studies A and C) with subjectively distributed plots of 40 m radius, within which we only used trees within a 10 m radius. These large plots allowed us to simulate the impact of position errors by perturbing the plot centers. Second, we also had access to a larger dataset of systematically distributed plots with 10 m radius (case studies B and D), which represent a common case in many remote sensing studies. In the following, we first present the assumptions related to the field reference errors (i.e., measurement errors, model errors and position errors), and then we present the remote sensing models used to generate the AGB predictions.

3.4.1. Field reference errors

The assumptions about measurement error magnitudes were based on the Swedish NFI control inventory. The variables most relevant for the current study (and possible future replications) from Fridman et al. (2019) are presented in Table 2. In the field inventories in the case study areas, the height (H) was only measured on a subset of trees within the

Table 2

Estimated bias and standard deviation (sd) in field measurements performed by the Swedish NFI, based on control inventory data 2012–2016 for common tree attributes used to estimate the AGB using a function. The number of sample trees is denoted by N.

Attribute	Unit	Min	Max	Mean	Bias	Sd	N
DBH	cm	4.0	63	34	0.082 (0.24%)	0.670 (0.19%)	9153
H	m	1.3	37	16	0.071 (0.45%)	0.575 (0.37%)	1957
ln(H)	ln(m)	2.6	5.9	5.0	−0.006 (−0.12%)	1.858 (0.37%)	1957

Table 3

Estimated variances in $[(\ln(kg))^2]$ of random errors at tree ($\hat{\sigma}_\tau^2$) and plot $\hat{\sigma}_\delta^2$ level obtained from the AGB model dataset.

Species	Tree level variance $\hat{\sigma}_\tau^2$	Plot level variance $\hat{\sigma}_\delta^2$
Pine	0.05071	0.01809
Spruce	0.05900681	0.01809
Birch	0.06007115	0.01809

plots, and we therefore decided to use the AGB functions that only require tree species and DBH as explanatory variables, which were measured on all trees. Thus, we assumed that all trees were properly found on each plot, and we only accounted for measurement errors occurring through diameter measurements.

The variances of the error terms δ_k and τ_{jk} were estimated using the dataset for which the AGB models were derived (Marklund, 1988). The AGB model parameters for pine (T1, stem, and T13, branches), spruce (G1, stem, and G11, branches) and birch (B1, stem, B11, branches) were estimated using a linear mixed model, implemented in R using the *nlme* package. The relation to AGB was defined as $ln(AGB) = \beta_0 + \beta_1 \frac{DBH}{DBH + constant_{species}}$ with the constants for the species pine, spruce and birch being 13, 14 and 8 respectively. The estimated variance of the error at plot level, $\hat{\sigma}_\delta^2$, and tree level, $\hat{\sigma}_\tau^2$, respectively, are presented in Table 3. According to our model assumptions, the estimator of the model parameter vector β was unbiased. The trees used to develop the biomass functions (Marklund, 1988) were measured very carefully and the measurement errors were very small. We therefore assumed that the measurement errors for the dataset used to develop the biomass functions had mean zero.

The position error of plots has a limited impact on the variance of R_1 (which is dominated by measurement errors) and R_2 (dominated by model errors), since they cause us to measure the trees on a wrongly positioned plot, but the measurements themselves are not affected by the incorrect position. However, a correct plot position is key when linking the measured attributes to other geospatial data, e.g., the remote sensing data.

We simulated perturbed plot center positions by adding an error with the magnitude expressed as DRMS, defined as (Devon et al., 2015; Yoshimura and Hasegawa, 2003)

$$DRMS = \sqrt{\sigma_E^2 + \sigma_N^2}, \tag{12}$$

where σ_E and σ_N denote the standard deviation of a normally distributed position error in the east and north directions, respectively. We simulated the impact of various position errors: DRMS = 0, 1, 5, and 10 m (where $\sigma_E = \sigma_N$). Then, we included the trees on the perturbed 10 m plot positions instead of the correct 10 m plots and quantified the impact. We assumed that the plot position error would not cause large parts of the plots to cross any stand borders, since large errors can normally be identified as outliers in the analysis. In our case, we used mirroring to overcome plot positions randomly falling outside the region we had tree data from (Kleinn and Vilčko, 2005). The forest conditions of the "large" plots were assumed to represent the order of magnitude of the respective errors well within the test sites. We therefore assumed the same order of residual errors when the systematic field plots were used in case study B and D, as for the subjectively chosen plots in case study A and C. Monte

Carlo simulations with 10,000 replications per plot were performed, and based on these, the expectations and variances of R_{1k}, R_{2k}, and R_{3k} as well as the covariance between R_{1k} and R_{3k} were computed for each plot. Then, the average expectation and variance over all plots were computed for each error type. The average covariance between R_{1k} and R_{3k} over all plots was also computed. The Monte Carlo procedure for computing unconditional expectations and variances can be summarized as:

1. Generate perturbed plot-centers assuming normally distributed errors in easting and northing.
2. Identify trees within the true and perturbed plots.
3. For each error type and plot, compute the expectation and variance conditioned on the position error.
4. Repeat the first three steps 10,000 times.
5. For each error type and plot, use the 10,000 replications to estimate the unconditional expectation and variance.
6. For each error type, compute the average expectation and variance over all plots.

A corresponding procedure was used for the covariance between R_{1k} and R_{3k}.

3.4.2. Processing of remote sensing data

The ALS data were normalized to represent heights above-ground using the software Lastools. Then, the following metrics were extracted as averages from each plot above a height cutoff of 1.37 m above ground: the height percentiles 10–90 (p10, p20, …, p90), p95, p99, max, average, average square height, standard deviation, skewness (ske), kurtosis (kur), canopy cover (the number of first returns above the cover cutoff divided by the number of all first returns), and canopy density (dns, the number of all points above the cover cutoff divided by the number of all returns). Since the plot averages were extracted directly from the point cloud, no edge effects were involved (as would happen if the point cloud would have been rasterized to pixels first).

3.4.3. Remote sensing models

Different regression models were developed in the four case studies to link the remote sensing data to the respective field references. For the case studies A and C, the number of plots were low (28 and 38 respectively, after removing outliers), and we therefore used a leave-one-out (LOO) approach to estimate the RS model parameters and generate the predictions using all plots but the one to be predicted. For the case studies B and D we had 349 and 219 plots available, respectively (Table 4). We considered this sufficient to split the datasets into halves, by first ordering the plots according to their AGB, and then assigning every second plot to training and validation datasets, respectively. The

Table 4

Regression model parameters. For case A and C (where LOO was used to estimate the parameters), the mean values from the n models are reported.

Case study	Test site	$\hat{\alpha}_0$	$\hat{\alpha}_1$	$\hat{\alpha}_2$	$\hat{\alpha}_3$	$\hat{\sigma}_\varepsilon$	n
A	Krycklan	−4.51	16.7	–	–	19.6	27
B	Krycklan	13.5	10.9	–	–	22.7	172
C	Remningstorp	42.7	0.00669	−0.992	2.54	24.5	37
D	Remningstorp	13.9	8.84	0.379	–	44.7	109

training dataset was used to estimate the RS model parameters, and the evaluation dataset was used to quantify the model performance. A few plots were considered as outliers and therefore removed.

For all four case studies, we estimated the uncorrected RMSE and bias using

$$\widehat{RMSE} = \sqrt{\frac{1}{n}\sum_{i=1}^{n}(\widehat{Y}_i - Y_i)^2}, \tag{13}$$

$$\widehat{Bias} = \frac{1}{n}\sum_{i=1}^{n}(\widehat{Y}_i - Y_i), \tag{14}$$

where Y_i denotes the reference value for plot i.

The regression models used in the four case studies (A-D) are presented in eqs. (15–18), with the estimated parameters listed in Table 4. Some high height percentile (e.g., $p95$) and a density metric (e.g. dns) were first tested in additive and multiplicative combinations. Then, all explanatory variables were tested and selected with regard to their statistical significance, their contribution to lowering the residual standard error, and their contribution to the adjusted R^2. Transformations of both the dependent and explanatory variables were tested to achieve a linear relationship to the references when this was not already the case and to obtain a homoscedastic error structure.

$$AGB = \alpha_0 + \alpha_1 p60 \bullet dns + \varepsilon, \tag{15}$$

$$AGB = \alpha_0 + \alpha_1 (p50 \bullet dns)^{1.25} + \varepsilon, \tag{16}$$

$$AGB = \alpha_0 + \alpha_1 (p30^3) + \alpha_2 ske + \alpha_3 p90\sqrt{kur} + \varepsilon, \tag{17}$$

$$AGB = \alpha_0 + \alpha_1 p30 + \alpha_2 p50^2 + \varepsilon, \tag{18}$$

where α_i, $i = \{0, 1, 2, 3\}$ denote the parameter values and ε denotes a random error.

We estimated the ECM parameters (λ_0, λ_1 and σ_ε) for each case study, and we adjusted for the measurement, model, and position errors that were estimated for each test site (as described in section 3.4.1). After the ECM parameters were estimated, we could estimate a corrected RMSE (5) and compare with the uncorrected RMSE (13).

4. Results

The results showed that the random errors in the field references were important to consider and affected the apparent accuracy of the RS-based predictions of AGB. In Section 4.1, we present the results of the error simulations, 4.2 presents the impact of the errors on the RS-based AGB predictions under the assumption of 1 m position error, and 4.3 presents results for different cases of larger position errors.

4.1. Estimates of error contributions

The estimated contribution of each error source and their sum are summarized in Tables 5 - 8. Measurement errors (R_{1k}) and model parameter errors (R_2) appeared as minor error sources compared to the position and residual model errors (R_3). The expectations were low for all three error types, although the small systematic measurement error was causing a systematic underestimation of the true AGB of about 1 t/ha, corresponding to <1% of the mean (Table 5). However, the variance of the residual errors (unexplained random model errors) due to using a model for predicting the AGB from DBH was large. Its impact can be quantified by comparing the variance of R_3 at a GNSS error = 0 m (no position error) with the corresponding variance for other position errors in Tables 6 and 8. In Krycklan, at 1 m GNSS error, the residual variance component constituted about 87% of the total variance, and the position error caused about 10% of the total variance (Table 6). In Remningstorp, the corresponding contributions were 80% (residual error) and 17% (position error).

Table 5
Summary of error expectation contributions in Krycklan, expressed as the mean over all plots at the test site. Plot values are presented in figures in Appendix A3. The error R_{1k} is dominated by measurement errors, R_{2k} by model parameter errors, and R_{3k} by a combination of position and residual model errors.

GNSS error [m]	Mean $E(R_{1k})$ [t/ha]	Mean $E(R_{2k})$ [t/ha]	Mean $E(R_{3k})$ [t/ha]	Sum [t/ha]
0	1.097	0	0	1.097
1	1.094	0	−0.3340	0.7599
5	1.083	0	−2.090	−1.007
10	1.063	0	−2.440	−1.374

Table 6
Summary of error variance contributions in Krycklan, expressed as the mean of all plots at the test site. Plot values are presented in figures in Appendix A3. The error R_1 is dominated by measurement errors, R_2 by model parameter errors, and R_3 by a combination of position and residual model errors.

GNSS error [m]	Mean Var (R_{1k}) [t^2/ha^2]	Mean Var (R_{2k}) [t^2/ha^2]	Mean Var (R_{3k}) [t^2/ha^2]	Mean 2Cov (R_{1k}, R_{3k}) [t^2/ha^2]	Sum [t^2/ha^2]
0	0.4835	0.01242	13.71	0	14.21
1	0.4828	0.01260	15.24	0.02316	15.76
5	0.4757	0.01258	23.25	0.1037	21.00
10	0.4741	0.01247	25.15	0.1853	25.82

Table 7
Summary of error expectation contributions in Remningstorp, expressed as the mean of all plots at the test site. Plot values are presented in figures in Appendix A.3. The error R_1 is dominated by measurement errors, R_2 by model parameter errors, and R_3 by a combination of position and residual model errors.

GNSS error [m]	Mean $E(R_{1k})$ [t/ha]	Mean $E(R_{2k})$ [t/ha]	Mean $E(R_{3k})$ [t/ha]	Sum [t/ha]
0	1.021	0	0	1.021
1	1.033	0	2.328	3.361
5	1.042	0	4.768	5.811
10	1.043	0	5.073	6.116

Table 8
Summary of error variance contributions in Remningstorp, expressed as the mean of all plots at the test site. Plot values are presented in figures in Appendix A.3. The error R_1 is dominated by measurement errors, R_2 by model parameter errors, and R_3 by a combination of position and residual model errors.

GNSS error [m]	Mean Var (R_1) [t^2/ha^2]	Mean Var (R_2) [t^2/ha^2]	Mean Var (R_3) [t^2/ha^2]	Mean 2Cov (R_1,R_3) [t^2/ha^2]	Sum [t^2/ha^2]
0	0.7113	0.04137	23.44	0	24.20
1	0.7223	0.04175	28.18	0.05133	29.00
5	0.7326	0.04241	39.31	0.1651	40.25
10	0.7354	0.04129	51.56	0.2901	52.63

Together, the model residuals and position inaccuracies greatly affected the interpretation of the accuracy of AGB predictions obtained from the RS model. Many previous studies have ignored the spatial correlation of trees within plots, which, however, was found to contribute substantially to the field reference errors in the present study. The residual model errors of trees decrease with increasing number of trees on a plot, which is not the case for the residual plot component since it is unique for each plot. Due to the magnitude of the plot component in Table 3 (which is on the same order as the tree level variance), this indicates that the effect of correlated errors for trees within plots has to be considered. The spatial error structure within the plots was not investigated and is one aspect to cover in future research. It
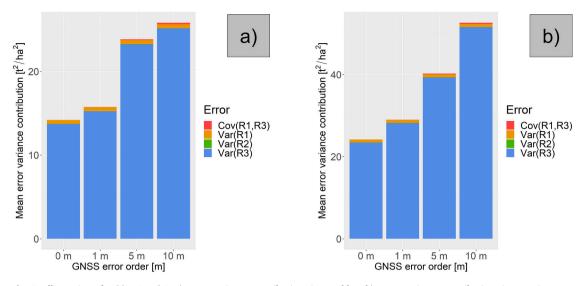
Fig. 3. Illustration of Tables 6 and 8. a) Error variance contributions in Krycklan. b) Error variance contributions in Remningstorp.

Table 9
Estimates for the ECM parameters (λ_0, λ_1, and σ_ε), RMSE and bias for the case studies.

Case study	Test site	$\widehat{\lambda}_0$	$\widehat{\lambda}_1$	$\widehat{\sigma}_\varepsilon$	RMSE [t/ha]	RMSE* [t/ha]	Bias [t/ha]	n
A	Krycklan	16.5	0.846	19.7	21.0 (19.3%)	19.8 (18.1%)	−0.277 (−0.254%)	28
B	Krycklan	11.9	0.859	18.7	20.6 (19.8%)	18.9 (18.1%)	−2.79 (−2.68%)	174
C	Remningstorp	35.7	0.777	23.3	26.0 (16.1%)	23.3 (14.4%)	−0.374 (−0.231%)	38
D	Remningstorp	41.3	0.689	35.6	43.4 (32.5%)	35.6 (26.7%)	−0.229 (−0.172%)	108

is likely that the plot size for which this effect can be seen reflects the type and size of forest at our test site, and that other regions would have this effect at other scales.

The errors related to position uncertainty of the plot locations were relatively influential and should thus be carefully considered in remote sensing studies. Depending on the measurement equipment for position (better than 1 m in our study) and on the plot location, the resulting uncertainty in AGB can vary substantially. For completeness, we investigated the effect for various common orders of position errors, as listed in Tables 5 – 8 and in Figs. 3. A plot position uncertainty on the order of 5 m has been rather common, although the combined use of the most recent GNSS systems can decrease the uncertainties. When the position accuracy decreases, they may only be paired with more inaccurate RS data sources providing less information (e.g., when using satellite images). A conclusion is that it is important to minimize position errors to increase the efficiency of RS data as auxiliary data source.

4.2. Impact on remote sensing-based AGB predictions

To address the first objective (describe the impact of field reference errors on the apparent accuracy of RS predictions), we estimated the ECM parameters, and the uncorrected and corrected RMSE, which we used as performance metrics. The ECM parameter estimates were relatively similar for both case study A and B, which both used the data located in Krycklan (Table 9, Figs. 4 a,b). This indicates that both the smaller (fewer subjective plots) and larger (systematic grid of plots) datasets represented the area well. The impact of the errors in the field references was 5.7% and 8.3% in the case studies A and B, respectively (Table 9). This corresponded to an RMSE that decreased from 19.3% to 18.1%, and 19.8% to 18.1% respectively (Table 9). The ECM parameter

estimates were slightly more different for the case studies C and D, which used data from Remningstorp. In particular, the residual error $\widehat{\sigma}_\varepsilon$ was about 50% higher in case study D compared to C. The impact of errors in the references was 10.6% and 17.8% in the case studies C and D, respectively. This corresponded to an RMSE that decreased from 16.1% to 14.4%, and 32.5% to 26.7%, respectively (Table 9, Figs. 4 c,d). The results are indicative for estimation of forest volume as well, which is closely related to AGB.

The average accuracy for different AGB values can be visualized with the error model (1) as shown in Fig. 5. The ECM enables the visualization of how the bias and precision changes across the range of AGB values, while the traditional accuracy metric RMSE indicates a constant accuracy, regardless of the AGB value. When comparing the ECM corrected accuracy with the uncorrected one, it can also be noticed that the ECM corrected has a narrower precision band due to the correction, this is particular obvious for the case D.

5. Discussion

The contribution from the different investigated error sources to the total variance of random errors in the field references varied substantially. We found that, in our case studies, the contributions from random measurement errors (R_1) and the uncertainty in the AGB model parameters (R_2) could in practice be ignored. On the other hand, the residual model errors tended to be large, and constituted in our case 80–87% of the total variance (Tables 6 and 8). An important reason for this was that we considered the intra-plot correlations of residual errors, which were found to occur in our empirical data (similar to findings by e.g., Breidenbach et al., 2014; Chave et al., 2004; Gregoire et al., 1995; Lehtonen et al., 2007; Repola, 2009). Studies ignoring this correlation
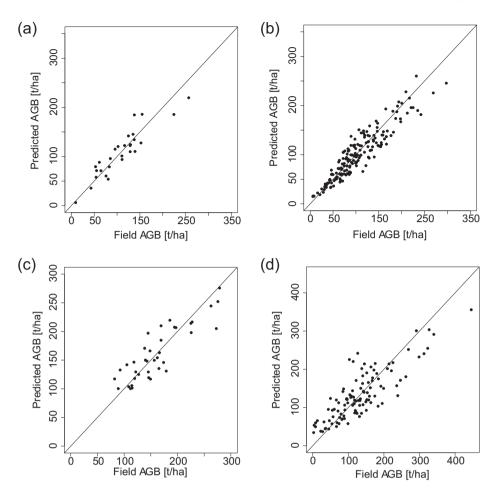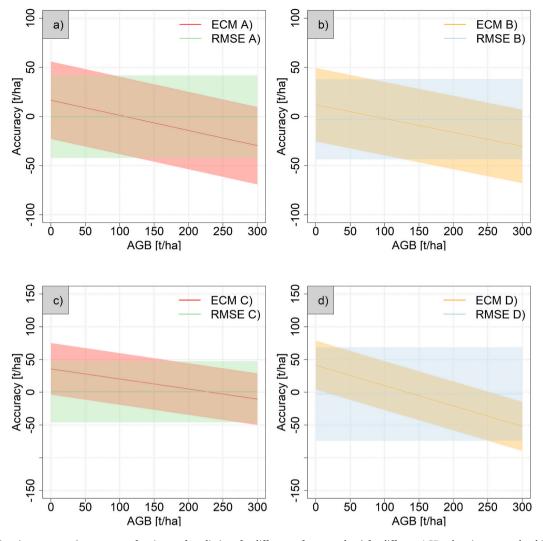
Fig. 4. AGB estimated from ALS and validated with reference AGB from the field. a,b) Krycklan (case study A, B). c,d) Remningstorp (case study C, D).

may underestimate the variance at plot- and stand-level. In case the residual errors would have been assumed to be independent, the residual error component would have been less influential. However, a problem in many studies is that researchers that use regional or national biomass models rarely have access to the original tree-level AGB model data, which are required for the computations we made in this study. The position errors were another influential error source (10–17% of the total variance at 1 m DRMS). The position errors can be reduced substantially (from tens of meters to sub meter) by using accurate GNSS positioning equipment, e.g., dGPS or RTK GPS, and locating the antenna higher above the ground to reduce interference effects. Thus, position errors on the order of magnitude of 1 m could be expected to be normal in future field inventories.

Although the measurement errors were small and their contribution to the total variance could practically be ignored, we identified a small systematic effect which should be considered. If different personnel or equipment are used for collecting training and evaluation data, this error may have a larger impact. The order of measurement errors were estimated for field personnel in the Swedish NFI, which are experienced in carrying out such inventories. With less experienced personnel, the variance may be larger. The small impact of measurement errors contradicts the findings by Chen et al. (2016) who listed tree attribute errors (denoted measurement errors in our study) as the second largest error source, almost as influential as the residual errors. However, they did

not have access to repeated measurements and could therefore not estimate this effect directly, but they had to assume the order of this error based on inventory tolerance limits. The impact of missed trees or counting trees twice were assumed small, but this error type was only measured as seedlings on circular plots with 1 m radius by the Swedish NFI and could therefore not be estimated properly. The Swedish NFI reported a failure of registering on average 0.16 trees (height < 1.3 m) per 1 m plot, and this number decreased to 0.01 trees when trees >1.3 m (but DBH < 4 cm) were considered (Fridman et al., 2019). The bottom line is that the procedure with manual measurements appeared to be sufficiently accurate for the RS applications. However, the Swedish NFI field protocols are very strict and the personnel usually well trained. In less controlled field inventories the measurement errors may be larger. Further, any systematic measurement errors will be the same in the field data used for model estimation and model evaluation, and thus such errors will not be observed in PRUC-based assessments.

The errors related to using a model for estimating the tree biomass are considerable. For larger areas, the uncertainty in the model parameters tend to dominate the error contribution, while at smaller, local areas, the residual model errors become increasingly important to consider (Chen et al., 2015, 2016; McRoberts, 2010; McRoberts et al., 2014b; McRoberts and Westfall, 2014). Within a single test site, where the same model parameters are used to estimate both the training and validation biomass, the parameter errors will in practice cancel out,

Fig. 5. a) The estimation accuracy (square-root of variance of predictions for different reference values) for different AGB values is expressed as bias (solid line) and precision (light band, ±2σ). The error characterization model (ECM) and RMSE illustrate accuracy differently across the range of AGB. a, b) Krycklan (case study A, B). c, d) Remningstorp (case study C, D).

given that they affect the entire biomass range similarly. Since we ordered the field plots according to their biomass and then assigned every second to training and validation, this effect was minimized (Table 6). In Appendix A3, Fig. F2 b, it can also be noted that the parameter errors are approximately the same across the entire biomass range, which further underlines that the model parameter errors will in practice cancel out within a test site when PRUC is applied.

Regional characteristics might make the tree level residuals correlated at certain geographical scales. If this correlation is strong within a study area, it would imply that plots used for model estimation and model evaluation would be similar with regard to this type of error, which would then be hidden in analyses based on PRUC. To investigate this we conducted a variance component analysis that enabled us to choose a residual model error form that was separated into two fractions: plot-level and tree-level variability. We found that especially the plot-level residual errors (common for all trees within a plot) were important to consider, while the effect of tree-level errors was milder. The latter is typically reduced significantly due to the appearance of

multiple trees per plot. Yet, this increases the impact of spatial correlation due to trees within a plot tend to be similar. It is often ignored due to the increased complexity and lack of empirical data. The biomass models we used were created from a sample of 1273 trees, which is fairly large for Swedish conditions, but this impact may not be representative for other regions or even noticed when using biomass models based on other, larger samples. The impact of the correlated tree errors on the residual model errors would therefore benefit from being repeated in other studies and at other locations, to possibly eliminate any impact of our specific set of empirical data. Additional studies are also required to further characterize the spatial tree correlation at various distances within plots and stands.

New inventory procedures that originate in RS techniques would benefit from new biomass models developed intentionally for being used with such metrics that can be obtained with RS. Plot-size and forest type are likely having a large impact on the within-plot modeling error, and this effect should therefore be addressed further for other forest types and other plot sizes.

The increased variance following position errors of field plots has previously been investigated in various settings, e.g., (McRoberts et al., 2018; Saarela et al., 2016), but when included and compared with other common field error sources, it became clear how important it is to reduce this effect. The impact was significant (constituted at least 10–17% of the total variance, Tables 5 – 8), and when working with RS data of high spatial precision (e.g., laser scanning), it is likely the single most important factor that in practice can be addressed and improved.

By considering the field induced errors when deriving the uncertainty of the RS-based predictions, the RS-related uncertainty decreased with 6–18% (1.2 to 5.8 percentage points, Table 9). The more accurate the RS-based predictions are, the more important it is to address the errors in the reference data. Currently, particularly laser-based and photo-based RS techniques would benefit from using the proposed ECM, and to consider the investigated reference data errors. This would mainly be due to the significantly higher positional accuracy for these techniques, compared to most moderate-resolution satellite-based ones. Persson and Ståhl (2020) discussed how the relation of random errors in the RS data and in the reference data (field) affect the apparent accuracy of RS-based predictions. They suggested that when the ratio of the standard deviation between them is <2, the reported RMSE is severely affected. In the current study, this ratio was about 5 (Tables 6, 8 and 9), and the field reference errors already had a considerable impact on the results.

The assumptions we used in this study appear reasonable given the forest and inventory procedures used in Scandinavia, but with other forest types and other equipment and personnel, the assumptions must be adjusted correspondingly. For example, the plot sizes should likely be adjusted to match the trees in the study area. Other types of trees and vegetation will also cause other levels of measurement errors and position errors. The position errors are likely to increase considerably as the canopy is closing, and in forest with higher basal area. This could have the impact that position errors become equally important as the residual model errors when trees within plots are correlated, when working in areas with higher biomass. However, if the plot sizes are increased to better match larger trees with higher biomass, the impact of position errors are reduced. How these effects interact needs to be further investigated.

The ECM is suitable to handle cases where the mean errors can be described by a simple linear model, assuming a homoscedastic error structure. However, if the errors are heteroscedastic, the ECM still provides valid results, although the width of uncertainty (the bands in Fig. 3) cannot be properly described across the range of biomass. This poses a possible extension to the current ECM in future studies.

The order of magnitude of the respective error source that were investigated in this study generally agrees with previous research (Berger et al., 2014; Gertner, 1990; Gertner and Köhl, 1992; McRoberts et al., 2018), but it was important to compare their effects on AGB predictions in the same study to rank their importance, and furthermore, to quantify their impact on the accuracy reported in RS studies using such reference data that are assumed true.

6. Conclusions

The paper addressed the impact of uncertainties in field reference data when used for training and evaluating plot level biomass estimates (or any other relevant variable of interest) in remote sensing studies based on pairwise comparisons at the level of typical assessment units.

The use of an ECM, proposed in Persson and Ståhl (2020), provided the framework to characterize, quantify, and estimate the impact of three common error sources: measurement errors, model errors, and position errors. Four conclusions were drawn from the study. First, field inventoried reference data are prone to such levels of errors, that the reported uncertainty of common RS-based predictions is significantly affected. In this study, the reported RMSE was reduced about 6–18%, by properly addressing the field reference errors. Second, the framework of using an error characterization model was useful for providing more details about the error structure of RS-based predictions, when their magnitude in terms of RMSE is known. It was demonstrated how three different error sources could be taken into account in correcting the parameter estimates of the ECM, since the ECM would otherwise have indicated an incorrect error structure. Third, the residual model errors related to using a function for estimating the biomass on the circular 10 m plots were severely affected by correlated tree-level residual errors. Most remote sensing studies do not have access to the necessary data to correct for this error source (those used for creating the biomass models), but nevertheless, it is important to acknowledge the presence of this error term. Furthermore, it should be prioritized to provide estimates of the variances of errors on both tree and plot level together with the biomass models, when such models are estimated in the future. Fourth, the position of field plots constituted a significant error source that increased rapidly with increased GNSS inaccuracies. This is also the most important error source that could be reduced in future studies, using modern GNSS equipment.

Authorship contributions

Henrik Jan Persson: Conceptualization, Methodology, Validation, Formal analysis, Investigation, Data curation, Writing - Original draft & Review & Editing, Visualization, Project administration, Funding acquisition

Magnus Ekström: Conceptualization, Methodology, Writing - original draft (Appendix A1 and A2), Writing - Review & Editing

Göran Ståhl: Conceptualization, Methodology, Writing - Review & Editing

Declaration of Competing Interest

The authors declare that they have no known competing financial interests or personal relationships that could have appeared to influence the work reported in this paper.

Data availability

Data will be made available on request.

Appendix A. Appendix

A.1. Derivation for one tree species

In this first part, we consider the case where we have only one tree species, and therefore only need one model function, $f(x_{jk}, \boldsymbol{\beta})$.

Let $\nabla_{\boldsymbol{\beta}} g(x_{jk}, \boldsymbol{\beta})$ denote the gradient vector with elements $\frac{\partial g(x_{jk}, \boldsymbol{\beta})}{\partial \beta_i}$, $i = 0, \ldots, p$. Likewise, let $\nabla_x g(x_{jk}, \boldsymbol{\beta})$ denote the gradient vector with elements $\frac{\partial g(x_{jk}, \boldsymbol{\beta})}{\partial x_{jkl}}$, $l = 1, \ldots, p$. From (6) and (7), by a Taylor approximation of $T_{\text{ref}, k}$, we see that

$$T_{\text{ref},k} \approx \sum_{j' \in M'_k} g(x_{j'k}, \boldsymbol{\beta}) exp(s_{j'k}) + \sum_{j' \in M'_k} \left\{ \sum_{l=1}^{p} \left(\widetilde{X}_{j'kl} - x_{j'kl} \right) \frac{\partial g(x_{j'k}, \boldsymbol{\beta})}{\partial x_{j'kl}} + \sum_{i=0}^{p} (\widehat{\beta}_i - \beta_i) \frac{\partial g(x_{j'k}, \boldsymbol{\beta})}{\partial \beta_i} \right\} exp(s_{j'k})$$

$$= T_k + \sum_{j \in M'_k \cap M_k} g(x_{jk}, \boldsymbol{\beta}) \left(exp(s_{jk}) - exp(\varepsilon_{jk}) \right) + \left\{ \sum_{j' \in M'_k \backslash M_k} g(x_{j'k}, \boldsymbol{\beta}) exp(s_{j'k}) - \sum_{j \in M_k \backslash M'_k} g(x_{jk}, \boldsymbol{\beta}) exp(\varepsilon_{jk}) \right\} + \sum_{j' \in M'_k} \left\{ \sum_{l=1}^{p} \eta_{j'kl} \frac{\partial g(x_{j'k}, \boldsymbol{\beta})}{\partial x_{j'kl}} + \sum_{i=0}^{p} (\widehat{\beta}_i - \beta_i) \frac{\partial g(x_{j'k}, \boldsymbol{\beta})}{\partial \beta_i} \right\} exp(s_{j'k}).$$

If we rewrite this expression, we get (8), i.e., $T_{ref, k} - T_k \approx R_{1k} + R_{2k} + R_{3k}$, where R_{ik}, $i = 1, 2, 3$, are defined in (9), (10), and (11), respectively.

Let $\Sigma_{\eta_{jk}}$ and $\Sigma_{\boldsymbol{\beta}}$ denote the covariance matrices of $\boldsymbol{\eta}_{jk}$ and $\boldsymbol{\beta}$, respectively. Given the position error ρ_k, R_{1k} and R_{2k} can be handled as in Gertner (1990). That is,

$$E(R_{1k}|\boldsymbol{\rho}_k) = \sum_{j' \in M'_k} exp(s_{j'k}) \left(\nabla_x g(x_{j'k}, \boldsymbol{\beta}) \right)^T E(\boldsymbol{\eta}_{j'k}),$$

$$Var(R_{1k}|\boldsymbol{\rho}_k) = \sum_{j' \in M'_k} exp(2s_{j'k}) \left(\nabla_x g(x_{j'k}, \boldsymbol{\beta}) \right)^T \Sigma_{\eta_{jk}} \nabla_x g(x_{j'k}, \boldsymbol{\beta}),$$

$$E(R_{2k}|\boldsymbol{\rho}_k) = \sum_{j' \in M'_k} exp(s_{j'k}) \left(\nabla_{\boldsymbol{\beta}} g(x_{j'k}, \boldsymbol{\beta}) \right)^T E(\widehat{\boldsymbol{\beta}} - \boldsymbol{\beta}),$$

and

$$Var(R_{2k}|\boldsymbol{\rho}_k) = \sum_{j' \in M'_k} exp(2s_{j'k}) \left(\nabla_{\boldsymbol{\beta}} g(x_{j'k}, \boldsymbol{\beta}) \right)^T \Sigma_{\boldsymbol{\beta}} \nabla_{\boldsymbol{\beta}} g(x_{j'k}, \boldsymbol{\beta}).$$

Corresponding unconditional expectations and variances can be obtained through the law of total expectation, $E(R_{ik}) = E(E(R_{ik}|\boldsymbol{\rho}_k))$, and the law of total variance, $Var(R_{ik}) = Var(E(R_{ik}|\boldsymbol{\rho}_k)) + E(Var(R_{ik}|\boldsymbol{\rho}_k))$, respectively. For computing these unconditional quantities, Monte Carlo simulations may be used.

Let us consider R_{3k}, and recall that $\varepsilon_{jk} = \delta_k + \tau_{jk}$. It is assumed that δ_k and τ_{jk} are independent random variables with mean zero and variances σ_δ^2 and σ_τ^2, respectively. Given the position error ρ_k, we get

$$E(R_{3k}|\boldsymbol{\rho}_k) = \sum_{j \in M'_k \cap M_k} g(x_{jk}, \boldsymbol{\beta}) E\left(exp(s_{jk}) - exp(\varepsilon_{jk}) \right) + \left\{ \sum_{j' \in M'_k \backslash M_k} g(x_{j'k}, \boldsymbol{\beta}) exp(s_{j'k}) - \sum_{j \in M_k \backslash M'_k} g(x_{jk}, \boldsymbol{\beta}) E(exp(\varepsilon_{jk})) \right\}$$

$$= \sum_{j' \in M'_k \backslash M_k} g(x_{j'k}, \boldsymbol{\beta}) exp(s_{j'k}) - \sum_{j \in M_k \backslash M'_k} g(x_{jk}, \boldsymbol{\beta}) exp(s_{jk}).$$

and

$$Var(R_{3k}|\boldsymbol{\rho}_k) = \sum_{i \in M_k} \sum_{j \in M_k} g(x_{ik}, \boldsymbol{\beta}) g(x_{jk}, \boldsymbol{\beta}) Cov\left(exp(\varepsilon_{ik}), exp(\varepsilon_{jk}) \right),$$

where

$$Cov\left(exp(\varepsilon_{jk}), exp(\varepsilon_{jk}) \right) = Cov\left(exp(\delta_k + \tau_{jk}), exp(\delta_k + \tau_{jk}) \right) = exp(\sigma_\tau^2 + \sigma_\delta^2) \left[exp(\sigma_\tau^2 + \sigma_\delta^2) - 1 \right]$$

and

$$Cov\left(exp(\varepsilon_{ik}), exp(\varepsilon_{jk}) \right) = Cov\left(exp(\delta_k + \tau_{ik}), exp(\delta_k + \tau_{jk}) \right) = exp(\sigma_\tau^2 + \sigma_\delta^2) \left[exp(\sigma_\delta^2) - 1 \right]$$

for all $i \neq j$. Thus,

$$Var(R_{3k}|\boldsymbol{\rho}_k) = Var\left(\sum_{j \in M_k} g(x_{jk}\boldsymbol{\beta}) exp(\varepsilon_{jk}) \right) = exp(\sigma_\tau^2 + \sigma_\delta^2) \left[exp(\sigma_\tau^2 + \sigma_\delta^2) - 1 \right] \sum_{j \in M_k} \left(g(x_{jk}\boldsymbol{\beta}) \right)^2 + exp(\sigma_\tau^2 + \sigma_\delta^2) \left[exp(\sigma_\delta^2) - 1 \right] \sum_{i \in M_k} \sum_{j \in M_k \text{ and } j \neq i} g(x_{ik}\boldsymbol{\beta}) g(x_{jk}\boldsymbol{\beta}).$$

The corresponding unconditional expected value and variance can be written as

$$E(R_{3k}) = E(E(R_{3k}|\boldsymbol{\rho}_k)) = E\left(\sum_{j' \in M'_k \backslash M_k} g(\boldsymbol{x}_{j'k}, \boldsymbol{\beta}) exp(s_{j'k}) - \sum_{j \in M_k \backslash M'_k} g(\boldsymbol{x}_{jk}, \boldsymbol{\beta}) exp(s_{jk}) \right) \tag{A1}$$

and

$$Var(R_{3k}) = Var(E(R_{3k}|\boldsymbol{\rho}_k)) + E(Var(R_{3k}|\boldsymbol{\rho}_k))$$

$$= Var\left(\sum_{j' \in M'_k \backslash M_k} g(\boldsymbol{x}_{j'k}\boldsymbol{\beta}) exp(s_{j'k}) - \sum_{j \in M_k \backslash M'_k} g(\boldsymbol{x}_{jk}\boldsymbol{\beta}) exp(s_{jk}) \right) + exp(\sigma_\tau^2 + \sigma_\delta^2) \left[exp(\sigma_\tau^2 + \sigma_\delta^2) - 1 \right] \sum_{j \in M_k} (g(\boldsymbol{x}_{jk}\boldsymbol{\beta}))^2 + exp(\sigma_\tau^2 + \sigma_\delta^2) \left[exp(\sigma_\delta^2) \right.$$

$$\left. - 1 \right] \sum_{i \in M_k} \sum_{j \in M_k \ and \ j \neq i} g(\boldsymbol{x}_{ik}\boldsymbol{\beta}) g(\boldsymbol{x}_{jk}\boldsymbol{\beta}). \tag{A2}$$

where the expected value on the right-hand side of (A1) and the variance on the right-hand side of (A2) can be computed using Monte Carlo simulations. Here it is the position error that is random, and this error determines which trees that belong to M'_k, and how M'_k relates to M_k.

In general, we have

$$E(T_{ref,k} - T_k) \approx E(R_{1k}) + E(R_{2k}) + E(R_{3k})$$

and

$$Var(T_{ref,k} - T_k) \approx Var(R_{1k}) + Var(R_{2k}) + Var(R_{3k}) + 2Cov(R_{1k}, R_{2k}) + 2Cov(R_{1k}, R_{3k}) + 2Cov(R_{2k}, R_{3k}).$$

Thus, in addition to what has already been derived, we also need to determine the covariance terms, and for doing that we use the law of total covariance,

$$Cov(R_{ik}, R_{jk}) = Cov(E(R_{ik}|\boldsymbol{\rho}_k), E(R_{jk}|\boldsymbol{\rho}_k)) + E(Cov(R_{ik}, R_{jk}|\boldsymbol{\rho}_k)).$$

We assume that $\{\eta_{jkl}\}$, $\{\widehat{\beta}_i\}$, and $\{\varepsilon_{jk}\}$ are independent sets of random variables. Then, R_{ik} and R_{jk} are conditionally independent given the position error ρ_k, for all $i, j = 1, 2, 3$, where $i \neq j$. Hence,

$$Cov(R_{ik}, R_{jk}) = Cov(E(R_{ik}|\boldsymbol{\rho}_k), E(R_{jk}|\boldsymbol{\rho}_k)),$$

and

$$Cov(E(R_{1k}|\boldsymbol{\rho}_k), E(R_{2k}|\boldsymbol{\rho}_k)) = Cov\left(\sum_{j' \in M'_k} exp(s_{j'k}) (\nabla_x g(\boldsymbol{x}_{j'k}, \boldsymbol{\beta}))^T E(\boldsymbol{\eta}_{j'k}), \sum_{j' \in M'_k} exp(s_{j'k}) (\nabla_\beta g(\boldsymbol{x}_{j'k}, \boldsymbol{\beta}))^T E(\widehat{\boldsymbol{\beta}} - \boldsymbol{\beta}) \right),$$

$$Cov(E(R_{1k}|\boldsymbol{\rho}_k), E(R_{3k}|\boldsymbol{\rho}_k)) = Cov\left(\sum_{j' \in M'_k} exp(s_{j'k}) (\nabla_x g(\boldsymbol{x}_{j'k}, \boldsymbol{\beta}))^T E(\boldsymbol{\eta}_{j'k}), \sum_{j' \in M'_k \backslash M_k} g(\boldsymbol{x}_{j'k}, \boldsymbol{\beta}) exp(s_{j'k}) - \sum_{j \in M_k \backslash M'_k} g(\boldsymbol{x}_{jk}, \boldsymbol{\beta}) exp(s_{jk}) \right),$$

and

$$Cov(E(R_{2k}|\boldsymbol{\rho}_k), E(R_{3k}|\boldsymbol{\rho}_k)) = Cov\left(\sum_{j' \in M'_k} exp(s_{j'k}) (\nabla_\beta g(\boldsymbol{x}_{j'k}, \boldsymbol{\beta}))^T E(\widehat{\boldsymbol{\beta}} - \boldsymbol{\beta}), \sum_{j' \in M'_k \backslash M_k} g(\boldsymbol{x}_{j'k}, \boldsymbol{\beta}) exp(s_{j'k}) - \sum_{j \in M_k \backslash M'_k} g(\boldsymbol{x}_{jk}, \boldsymbol{\beta}) exp(s_{jk}) \right),$$

which all can be computed using Monte Carlo simulations.

A.2. Derivation for multiple tree species

In this second part, we consider the case where we have more than one tree species. In this more general case, the bias correction s_{jk}, the functions f and g, the parameter vectors $\boldsymbol{\beta}$ and $\widehat{\boldsymbol{\beta}}$, and the model for ε_{jk} will be different for different tree species. Except for $Var(R_{3k}|\rho_k)$, the generalization is straightforward. Therefore, below we focus on $Var(R_{3k}|\rho_k)$.

Let us consider the case when we have two tree species, a and b. Then,

$$Var(R_{3k}|\boldsymbol{\rho}_k) = \sum_{i\in M_k^{(a)}}\sum_{j\in M_k^{(a)}} g^{(a)}\left(\boldsymbol{x}_{ik},\boldsymbol{\beta}^{(a)}\right)g^{(a)}\left(\boldsymbol{x}_{jk},\boldsymbol{\beta}^{(a)}\right)Cov\left(exp\left(\varepsilon_{ik}^{(a)}\right),exp\left(\varepsilon_{jk}^{(a)}\right)\right) + 2\sum_{i\in M_k^{(a)}}\sum_{j\in M_k^{(b)}} g^{(a)}\left(\boldsymbol{x}_{ik},\boldsymbol{\beta}^{(a)}\right)g^{(b)}\left(\boldsymbol{x}_{jk},\boldsymbol{\beta}^{(b)}\right)Cov\left(exp\left(\varepsilon_{ik}^{(a)}\right),exp\left(\varepsilon_{jk}^{(b)}\right)\right)$$
$$+ \sum_{i\in M_k^{(b)}}\sum_{j\in M_k^{(b)}} g^{(b)}\left(\boldsymbol{x}_{ik},\boldsymbol{\beta}^{(b)}\right)g^{(b)}\left(\boldsymbol{x}_{jk},\boldsymbol{\beta}^{(b)}\right)Cov\left(exp\left(\varepsilon_{ik}^{(b)}\right),exp\left(\varepsilon_{jk}^{(b)}\right)\right).$$

Assume that $\varepsilon_{jk}^{(a)} = \delta_k + \tau_{jk}^{(a)}$ and $\varepsilon_{jk}^{(b)} = \delta_k + \tau_{jk}^{(b)}$, where δ_k, $\tau_{jk}^{(a)}$, and $\tau_{jk}^{(b)}$ are independent. Then we get

$$Cov\left(exp\left(\varepsilon_{jk}^{(a)}\right),exp\left(\varepsilon_{jk}^{(a)}\right)\right) = Cov\left(exp\left(\delta_k + \tau_{jk}^{(a)}\right),exp\left(\delta_k + \tau_{jk}^{(a)}\right)\right) = exp(\sigma_{\tau^{(a)}}^2 + \sigma_\delta^2)\left[exp(\sigma_{\tau^{(a)}}^2 + \sigma_\delta^2) - 1\right]$$

and

$$Cov\left(exp\left(\varepsilon_{ik}^{(a)}\right),exp\left(\varepsilon_{jk}^{(a)}\right)\right) = Cov\left(exp\left(\delta_k + \tau_{ik}^{(a)}\right),exp\left(\delta_k + \tau_{jk}^{(a)}\right)\right) = exp(\sigma_{\tau^{(a)}}^2 + \sigma_\delta^2)\left[exp(\sigma_\delta^2) - 1\right]$$

for all $i \neq j$. Likewise, for species b we get

$$Cov\left(exp\left(\varepsilon_{jk}^{(b)}\right),exp\left(\varepsilon_{jk}^{(b)}\right)\right) = Cov\left(exp\left(\delta_k + \tau_{jk}^{(b)}\right),exp\left(\delta_k + \tau_{jk}^{(b)}\right)\right) = exp(\sigma_{\tau^{(b)}}^2 + \sigma_\delta^2)\left[exp(\sigma_{\tau^{(b)}}^2 + \sigma_\delta^2) - 1\right]$$

and

$$Cov\left(exp\left(\varepsilon_{ik}^{(b)}\right),exp\left(\varepsilon_{jk}^{(b)}\right)\right) = Cov\left(exp\left(\delta_k + \tau_{ik}^{(b)}\right),exp\left(\delta_k + \tau_{jk}^{(b)}\right)\right) = exp(\sigma_{\tau^{(b)}}^2 + \sigma_\delta^2)\left[exp(\sigma_\delta^2) - 1\right]$$

for all $i \neq j$. In addition,

$$Cov\left(exp\left(\varepsilon_{ik}^{(a)}\right),exp\left(\varepsilon_{jk}^{(b)}\right)\right) = Cov\left(exp\left(\delta_k + \tau_{ik}^{(a)}\right),exp\left(\delta_k + \tau_{jk}^{(b)}\right)\right) = exp\left(\frac{\sigma_{\tau^{(a)}}^2 + \sigma_{\tau^{(b)}}^2}{2} + \sigma_\delta^2\right)\left[exp(\sigma_\delta^2) - 1\right].$$

Thus,

$$E(Var(R_{3k}|\boldsymbol{\rho}_k)) = Var(R_{3k}|\boldsymbol{\rho}_k)$$
$$= exp(\sigma_{\tau^{(a)}}^2 + \sigma_\delta^2)\left[exp(\sigma_{\tau^{(a)}}^2 + \sigma_\delta^2) - 1\right]\sum_{j\in M_k^{(a)}}\left(g^{(a)}\left(\boldsymbol{x}_{jk}\boldsymbol{\beta}^{(a)}\right)\right)^2 + exp(\sigma_{\tau^{(a)}}^2 + \sigma_\delta^2)\left[exp(\sigma_\delta^2) - 1\right]\sum_{i\in M_k^{(a)}}\sum_{j\in M_k^{(a)}\ and\ j\neq i} g^{(a)}\left(\boldsymbol{x}_{ik}\boldsymbol{\beta}^{(a)}\right)g^{(a)}\left(\boldsymbol{x}_{jk}\boldsymbol{\beta}^{(a)}\right) + exp(\sigma_{\tau^{(b)}}^2$$
$$+ \sigma_\delta^2)\left[exp(\sigma_{\tau^{(b)}}^2 + \sigma_\delta^2) - 1\right]\sum_{j\in M_k^{(b)}}\left(g^{(b)}\left(\boldsymbol{x}_{jk}\boldsymbol{\beta}^{(b)}\right)\right)^2 + exp(\sigma_{\tau^{(b)}}^2 + \sigma_\delta^2)\left[exp(\sigma_\delta^2) - 1\right]\sum_{i\in M_k^{(b)}}\sum_{j\in M_k^{(b)}\ and\ j\neq i} g^{(b)}\left(\boldsymbol{x}_{ik}\boldsymbol{\beta}^{(b)}\right)g^{(b)}\left(\boldsymbol{x}_{jk}\boldsymbol{\beta}^{(b)}\right) + 2exp\left(\frac{\sigma_{\tau^{(a)}}^2 + \sigma_{\tau^{(b)}}^2}{2}\right)$$
$$+ \sigma_\delta^2\right)\left[exp(\sigma_\delta^2) - 1\right]\sum_{i\in M_k^{(a)}}\sum_{j\in M_k^{(b)}} g^{(a)}\left(\boldsymbol{x}_{ik}\boldsymbol{\beta}^{(a)}\right)g^{(b)}\left(\boldsymbol{x}_{jk}\boldsymbol{\beta}^{(b)}\right).$$

In case of three tree species, a, b, and c, we get

$$E(Var(R_{3k}|\boldsymbol{\rho}_k)) = Var(R_{3k}|\boldsymbol{\rho}_k)$$
$$= exp(\sigma_{\tau^{(a)}}^2 + \sigma_\delta^2)\left[exp(\sigma_{\tau^{(a)}}^2 + \sigma_\delta^2) - 1\right]\sum_{j\in M_k^{(a)}}\left(g^{(a)}\left(\boldsymbol{x}_{jk}\boldsymbol{\beta}^{(a)}\right)\right)^2 + exp(\sigma_{\tau^{(a)}}^2 + \sigma_\delta^2)\left[exp(\sigma_\delta^2) - 1\right]\sum_{i\in M_k^{(a)}}\sum_{j\in M_k^{(a)}\ and\ j\neq i} g^{(a)}\left(\boldsymbol{x}_{ik}\boldsymbol{\beta}^{(a)}\right)g^{(a)}\left(\boldsymbol{x}_{jk}\boldsymbol{\beta}^{(a)}\right) + exp(\sigma_{\tau^{(b)}}^2$$
$$+ \sigma_\delta^2)\left[exp(\sigma_{\tau^{(b)}}^2 + \sigma_\delta^2) - 1\right]\sum_{j\in M_k^{(b)}}\left(g^{(b)}\left(\boldsymbol{x}_{jk}\boldsymbol{\beta}^{(b)}\right)\right)^2 + exp(\sigma_{\tau^{(b)}}^2 + \sigma_\delta^2)\left[exp(\sigma_\delta^2) - 1\right]\sum_{i\in M_k^{(b)}}\sum_{j\in M_k^{(b)}\ and\ j\neq i} g^{(b)}\left(\boldsymbol{x}_{ik}\boldsymbol{\beta}^{(b)}\right)g^{(b)}\left(\boldsymbol{x}_{jk}\boldsymbol{\beta}^{(b)}\right) + exp(\sigma_{\tau^{(c)}}^2$$
$$+ \sigma_\delta^2)\left[exp(\sigma_{\tau^{(c)}}^2 + \sigma_\delta^2) - 1\right]\sum_{j\in M_k^{(c)}}\left(g^{(c)}\left(\boldsymbol{x}_{jk}\boldsymbol{\beta}^{(c)}\right)\right)^2 + exp(\sigma_{\tau^{(c)}}^2 + \sigma_\delta^2)\left[exp(\sigma_\delta^2) - 1\right]\sum_{i\in M_k^{(c)}}\sum_{j\in M_k^{(c)}\ and\ j\neq i} g^{(c)}\left(\boldsymbol{x}_{ik}\boldsymbol{\beta}^{(c)}\right)g^{(c)}\left(\boldsymbol{x}_{jk}\boldsymbol{\beta}^{(c)}\right) + 2exp\left(\frac{\sigma_{\tau^{(a)}}^2 + \sigma_{\tau^{(b)}}^2}{2}\right)$$
$$+ \sigma_\delta^2\right)\left[exp(\sigma_\delta^2) - 1\right]\sum_{i\in M_k^{(a)}}\sum_{j\in M_k^{(b)}} g^{(a)}\left(\boldsymbol{x}_{ik}\boldsymbol{\beta}^{(a)}\right)g^{(b)}\left(\boldsymbol{x}_{jk}\boldsymbol{\beta}^{(b)}\right) + 2exp\left(\frac{\sigma_{\tau^{(a)}}^2 + \sigma_{\tau^{(c)}}^2}{2} + \sigma_\delta^2\right)\left[exp(\sigma_\delta^2) - 1\right]\sum_{i\in M_k^{(a)}}\sum_{j\in M_k^{(c)}} g^{(a)}\left(\boldsymbol{x}_{ik}\boldsymbol{\beta}^{(a)}\right)g^{(c)}\left(\boldsymbol{x}_{jk}\boldsymbol{\beta}^{(c)}\right)$$
$$+ 2exp\left(\frac{\sigma_{\tau^{(b)}}^2 + \sigma_{\tau^{(c)}}^2}{2} + \sigma_\delta^2\right)\left[exp(\sigma_\delta^2) - 1\right]\sum_{i\in M_k^{(b)}}\sum_{j\in M_k^{(c)}} g^{(b)}\left(\boldsymbol{x}_{ik}\boldsymbol{\beta}^{(b)}\right)g^{(c)}\left(\boldsymbol{x}_{jk}\boldsymbol{\beta}^{(c)}\right).$$

A.3. Variance results for single plots

In this section we present some additional results for single plots, hence providing illustrations of and enabling a graphical representation (Figs. F1-F2) of the errors in relation to the reference biomass.
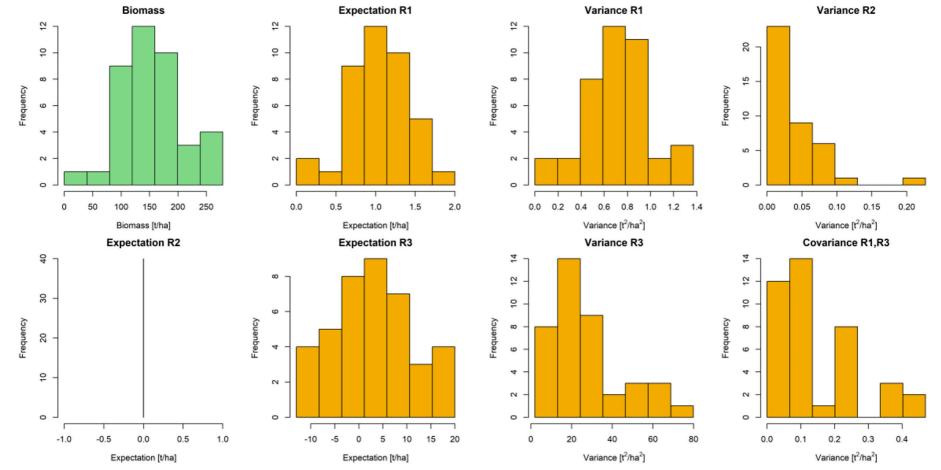
Fig. F1. Histograms for (left) the expectation and (right) variance of the error types in Remningstorp, assuming 1 m position uncertainty.
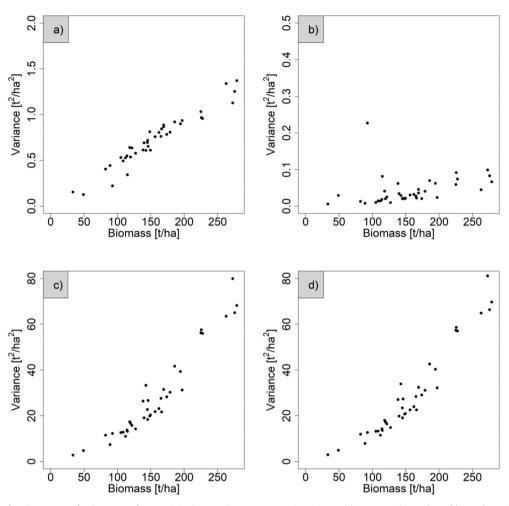
Fig. F2. Scatter plots of variance contributions vs. reference AGB in Remningstorp, assuming 1 m position uncertainty. A) R_1, b) R_2, c) R_3, d) Sum of all variance contributions.

References

Beck, J.V., Arnold, K.J., 1977. Parameter Estimation in Engineering and Science. John Wiley & Sons, New York.

Berger, A., Gschwantner, T., McRoberts, R.E., Schadauer, K., 2014. Effects of measurement errors on individual tree stem volume estimates for the Austrian national forest inventory. For. Sci. 60, 14–24. https://doi.org/10.5849/forsci.12-164.

Berglund, G., 2000. Jämförande studie : GPS-mätningar i skog. Uppsala, Sweden.

Berry, W.D., Feldman, S., 1985. Multiple Regression in Practice. https://doi.org/10.4135/9781412985208.

Breidenbach, J., Anton-Fernandez, C., Petersson, H., McRoberts, R.E., Astrup, R., 2014. Quantifying the model-related variability of biomass stock and change estimates in the Norwegian national forest inventory. For. Sci. 60, 25–33. https://doi.org/10.5849/forsci.12-137.

Broman, N., Christoffersson, J., 1999. Mätfel i provträdsvariabler och dess inverkan på precision och noggrannhet i volymskattningar. Umeå, Sweden.

Buonaccorsi, J.P., 2010. Measurement Error. Models, methods and applications. CRC Press.

Carroll, R.J., Ruppert, D., Stefanski, L.A., Crainiceanu, C., 2006. Measurement Error in Nonlinear Models: A Modern Perspective, Second. ed. Chapman and Hall.

Chave, J., Condit, R., Aguilar, S., Hernandez, A., Lao, S., Perez, R., 2004. Error propagation and sealing for tropical forest biomass estimates. In: Philosophical Transactions of the Royal Society B: Biological Sciences. Royal Society, pp. 409–420. https://doi.org/10.1098/rstb.2003.1425.

Chen, Q., Vaglio Laurin, G., Valentini, R., 2015. Uncertainty of remotely sensed aboveground biomass over an African tropical forest: propagating errors from trees to plots to pixels. Remote Sens. Environ. 160, 134–143. https://doi.org/10.1016/j.rse.2015.01.009.

Chen, Q., McRoberts, R.E., Wang, C., Radtke, P.J., 2016. Forest aboveground biomass mapping and estimation across multiple spatial scales using model-based inference. Remote Sens. Environ. 184, 350–360. https://doi.org/10.1016/j.rse.2016.07.023.

Chin, G.Y., 1987. Two-Dimensional Measures of Accuracy in Navigational Systems. Cambridge.

Clifford, D., Cressie, N., England, J.R., Roxburgh, S.H., Paul, K.I., 2013. Correction factors for unbiased, efficient estimation and prediction of biomass from log-log allometric models. For. Ecol. Manag. 310, 375–381. https://doi.org/10.1016/j.foreco.2013.08.041.

Coulston, J.W., Reams, G.A., McRoberts, E.R., Smith, W.D., 2004. Practical considerations when using perturbed forest inventory plot locations to develop spatial models: a case study. In: Forest Inventory and Analysis Symposium, pp. 81–86, 21-24 Sep., Denver, CO, USA.

de Lera Garrido, A., Gobakken, T., Ørka, H.O., Næsset, E., Bollandsås, O.M., 2020. Reuse of field data in als-assisted forest inventory. Silva Fenn. 54, 1–18. https://doi.org/10.14214/sf.10272.

DeCesare, N.J., Squires, J.R., Kolbe, J.A., 2005. Effect of forest canopy on GPS-based movement data. Wildl. Soc. Bull. 33, 935–941. https://doi.org/10.2193/0091-7648(2005)33[935:eofcog]2.0.co;2.

Devon, D., Holzer, T., Sarkani, S., 2015. Minimizing uncertainty and improving accuracy when fusing multiple stationary GPS receivers. In: IEEE International Conference on Multisensor Fusion and Integration for Intelligent Systems, pp. 83–88. https://doi.org/10.1109/MFI.2015.7295750, 14-15 Sep, San Diego, USA.

Ekström, M., Nilsson, M., 2021. A comparison of model-assisted estimators, with and without data-driven transformations of auxiliary variables, with application to forest inventory. Front. For. Glob. Chang. 4, 1–13. https://doi.org/10.3389/ffgc.2021.764495.

Ekström, M., Esseen, P.A., Westerlund, B., Grafström, A., Jonsson, B.G., Ståhl, G., 2018. Logistic regression for clustered data from environmental monitoring programs. Ecol. Inform. 43, 165–173. https://doi.org/10.1016/j.ecoinf.2017.10.006.

Fonseca, J.R., Friswell, M.I., Mottershead, J.E., Lees, A.W., 2005. Uncertainty identification by the maximum likelihood method. J. Sound Vib. 288, 587–599. https://doi.org/10.1016/j.jsv.2005.07.006.

Fox, J.C., Ades, P.K., Bi, H., 2001. Stochastic structure and individual-tree growth models. For. Ecol. Manag. 154, 261–276. https://doi.org/10.1016/S0378-1127(00)00632-0.

Frair, J.L., Fieberg, J., Hebblewhite, M., Cagnacci, F., DeCesare, N.J., Pedrotti, L., 2010. Resolving issues of imprecise and habitat-biased locations in ecological analyses

using GPS telemetry data. Philos. Trans. R. Soc. B Biol. Sci. 365, 2187–2200. https://doi.org/10.1098/rstb.2010.0084.

Frazer, G.W., Magnussen, S., Wulder, M.A., Niemann, K.O., 2011. Simulated impact of sample plot size and co-registration error on the accuracy and uncertainty of LiDAR-derived estimates of forest stand biomass. Remote Sens. Environ. 115, 636–649. https://doi.org/10.1016/j.rse.2010.10.008.

Friberg, G., Jönsson, P., 2012. Kontroll av noggrannheten av GPS-positionering hos skördare nr. 778–2012. Uppsala, Sweden.

Fridman, J., Holm, S., Nilsson, M., Nilsson, P., 2014. Adapting National Forest Inventories to changing requirements–the case of the Swedish National Forest Inventory at the turn of the 20th century. Silva Fenn. 48, 1–29.

Fridman, J., Wulff, S., Dahlgren, J., 2019. Resultat från kontrolltaxering av Riksskogstaxeringens datainsamling 2012-2016. Umeå, Sweden.

Fuller, W.A., 1987. Measurement Error Models, First. ed. John Wiley & Sons, New York.

Galán, C.O., Rodríguez-pérez, J.R., Torres, J.M., Nieto, P.J.G., 2011. Analysis of the influence of forest environments on the accuracy of GPS measurements by using genetic algorithms. Math. Comput. Model. 54, 1829–1834. https://doi.org/10.1016/j.mcm.2010.11.077.

Gertner, G.Z., 1986. Postcalibration sensitivity procedure for regressor variable errors. Can. J. For. Res. 16, 1120–1123.

Gertner, G.Z., 1987. Approximating precision in simulation projections: an efficient alternative to Monte Carlo methods. For. Sci. 33, 230–239.

Gertner, G.Z., 1990. The sensitivity of measurement error in stand volume estimation. Can. J. For. Res. 20, 800–804.

Gertner, G.Z., Köhl, M., 1992. An assessment of some nonsampling errors in a national survey using an error budget. For. Sci. 38, 525–538. https://doi.org/10.1093/forestscience/38.3.525.

Gregoire, T.G., Schabenberger, O., Barrett, J.P., 1995. Linear modelling of irregularly spaced, unbalanced, longitudinal data from permanent-plot measurements. Can. J. For. Res. 25, 20.

Gregoire, T.G., Næsset, E., McRoberts, R.E., Ståhl, G., Andersen, H.E., Gobakken, T., Ene, L., Nelson, R., 2016. Statistical rigor in LiDAR-assisted estimation of aboveground forest biomass. Remote Sens. Environ. 173, 98–108. https://doi.org/10.1016/j.rse.2015.11.012.

Hernández-Stefanoni, J.L., Reyes-Palomeque, G., Castillo-Santiago, Ángel, M., George-Chacón, S.P., Huechacona-Ruiz, A.H., Tun-Dzul, F., Rondon-Rivera, D., Dupuy, J.M., 2018. Effects of sample plot size and GPS location errors on aboveground biomass estimates from LiDAR in tropical dry forests. Remote Sens. 10, 1–15. https://doi.org/10.3390/rs10101586.

Hyyppä, J., Hyyppä, H., Inkinen, M., Engdahl, M., Linko, S., Zhu, Y.-H.H., Hyyppa, J., Hyyppa, H., Inkinen, M., Engdahl, M., Linko, S., Zhu, Y.-H.H., 2000. Accuracy comparison of various remote sensing data sources in the retrieval of forest stand attributes. For. Ecol. Manag. 128, 109–120. https://doi.org/10.1016/S0378-1127(99)00278-9.

Johansson, S., 2019. Korståg mot dåliga positioner. Skogforsk Vis. 20–23.

Jucker, T., Caspersen, J., Chave, J., Antin, C., Barbier, N., Bongers, F., Dalponte, M., van Ewijk, K.Y., Forrester, D.I., Haeni, M., Higgins, S.I., Holdaway, R.J., Iida, Y., Lorimer, C., Marshall, P.L., Momo, S., Moncrieff, G.R., Ploton, P., Poorter, L., Rahman, K.A., Schlund, M., Sonké, B., Sterck, F.J., Trugman, A.T., Usoltsev, V.A., Vanderwel, M.C., Waldner, P., Wedeux, B.M.M., Wirth, C., Wöll, H., Woods, M., Xiang, W., Zimmermann, N.E., Coomes, D.A., 2017. Allometric equations for integrating remote sensing imagery into forest monitoring programmes. Glob. Chang. Biol. 23, 177–190. https://doi.org/10.1111/gcb.13388.

Kendall, M., Stuart, A., Ord, J., 1987. Kendall's Advanced Theory of Statistics, Vol. 1. ed. Oxford Univ Press, New York.

Kleinn, C., Vilčko, F., 2005. Ein Vergleich von zwei methodischen Konzepten für die Grundgesamtheit von Probeflächen bei Waldinventuren. Allg. Forst- und Jagdzeitung 176, 68–74.

Lee, E., Forthofer, R., 2006. Analyzing Complex Survey Data. https://doi.org/10.4135/9781412983341.

Lehtonen, A., Cienciala, E., Tatarinov, F., Mäkipää, R., 2007. Uncertainty estimation of biomass expansion factors for Norway spruce in the Czech Republic. Ann. For. Sci. 64, 133–140.

Marklund, L.G., 1987. Biomass functions for Norway spruce (Picea abies (L.) Karst.). In: Sweden. Swedish University of Agricultural Sciences, Umeå, Sweden.

Marklund, L.G., 1988. Biomassafunktioner för tall, gran och björk i Sverige. Umeå, Sweden.

Mauya, E.W., Hansen, E.H., Gobakken, T., Bollandsås, O.M., Malimbwi, R.E., Næsset, E., 2015. Effects of field plot size on prediction accuracy of aboveground biomass in airborne laser scanning-assisted inventories in tropical rain forests of Tanzania. Carbon Balance Manag. 10 https://doi.org/10.1186/s13021-015-0021-x.

McRoberts, R.E., 2006. A model-based approach to estimating forest area. Remote Sens. Environ. 103, 56–66. https://doi.org/10.1016/j.rse.2006.03.005.

McRoberts, R.E., 2010. Probability- and model-based approaches to inference for proportion forest using satellite imagery as ancillary data. Remote Sens. Environ. 114 https://doi.org/10.1016/j.rse.2009.12.013.

McRoberts, R.E., Westfall, J.A., 2014. Effects of uncertainty in model predictions of individual tree volume on large area volume estimates. For. Sci. 60 https://doi.org/10.5849/forsci.12-141.

McRoberts, R.E., Holden, G.R., Nelson, M.D., Liknes, G.C., Moser, W.K., Lister, A.J., King, S.L., LaPoint, E.B., Coulston, J.W., Smith, W.B., Reams, G.A., 2005. Estimating and circumventing the effects of perturbing and swapping inventory plot locations. J. For. 103, 275–279. https://doi.org/10.1093/jof/103.6.275.

McRoberts, R.E., Tomppo, E.O., Finley, A.O., Heikkinen, J., 2007. Estimating areal means and variances of forest attributes using the k-Nearest Neighbors technique

and satellite imagery. Remote Sens. Environ. 111, 466–480. https://doi.org/10.1016/j.rse.2007.04.002.

McRoberts, R.E., Cohen, W.B., Næsset, E., Stehman, S.V., Tomppo, E.O., 2010. Using remotely sensed data to construct and assess forest attribute maps and related spatial products. Scand. J. For. Res. 25, 340–367. https://doi.org/10.1080/02827581.2010.497496.

McRoberts, R.E., Andersen, H.-E., Næsset, E., 2014a. Using airborne laser scanning data to support forest sample surveys. In: Maltamo, M., Næsset, E., Vauhkonen, J. (Eds.), Forestry Applications of Airborne Laser Scanning: Concepts and Case Studies. Springer, Netherlands, Dordrecht, pp. 269–292. https://doi.org/10.1007/978-94-017-8663-8_14.

McRoberts, R.E., Næsset, E., Gobakken, T., 2014b. Estimation for inaccessible and non-sampled forest areas using model-based inference and remotely sensed auxiliary information. Remote Sens. Environ. 154, 226–233. https://doi.org/10.1016/j.rse.2014.08.028.

McRoberts, R.E., Chen, Q., Domke, G.M., Ståhl, G., Saarela, S., Westfall, J.A., 2016. Hybrid estimators for mean aboveground carbon per unit area. For. Ecol. Manag. 378, 44–56. https://doi.org/10.1016/j.foreco.2016.07.007.

McRoberts, R.E., Chen, Q., Walters, B.F., Kaisershot, D.J., 2018. The effects of global positioning system receiver accuracy on airborne laser scanning-assisted estimates of aboveground biomass. Remote Sens. Environ. 207, 42–49. https://doi.org/10.1016/j.rse.2017.09.036.

Meng, S.X., Huang, S., 2010. Incorporating correlated error structures into mixed forest growth models: prediction and inference implications. Can. J. For. Res. 40, 977–990. https://doi.org/10.1139/X10-032.

Næsset, E., 2004a. Accuracy of forest inventory using airborne laser scanning: evaluating the first nordic full-scale operational project. Scand. J. For. Res. 19, 554–557. https://doi.org/10.1080/02827580410019544.

Næsset, E., 2004b. Practical large-scale forest stand inventory using a small-footprint airborne scanning laser. Scand. J. For. Res. 19, 164–179. https://doi.org/10.1080/02827580310019257.

Næsset, E., Gjevestad, J.G., 2008. Performance of GPS precise point positioning under conifer forest canopies. Photogramm. Eng. Remote Sens. 74, 661–668. https://doi.org/10.14358/PERS.74.5.661.

Næsset, E., Gobakken, T., 2008. Estimation of above- and below-ground biomass across regions of the boreal forest zone using airborne laser. Remote Sens. Environ. 112, 3079–3090. https://doi.org/10.1016/j.rse.2008.03.004.

Nilsson, M., 1997. Estimation of Forest Variables Using Satellite Image Data and Airborne Lidar. Doctoral Thesis. Swedish University of Agricultural Sciences.

NovAtel, 2003. GPS Position Accuracy Measures. APN-029 Rev 1.

Parresol, B.R., 1999. Assessing tree and stand biomass: a review with examples and critical comparisons. For. Sci. 45, 573–593. https://doi.org/10.1093/forestscience/45.4.573.

Persson, H., Fransson, J.E.S., 2014. Forest variable estimation using radargrammetric processing of TerraSAR-X images in boreal forests. Remote Sens. 6, 2084–2107. https://doi.org/10.3390/rs6032084.

Persson, H.J., Fransson, J.E.S., 2017. Comparison between TanDEM-X and ALS based estimation of above ground biomass and tree height in boreal forests. Scand. J. For. Res. 32, 306–319. https://doi.org/10.1080/02827581.2016.1220618.

Persson, H.J., Ståhl, G., 2020. Characterizing uncertainty in forest remote sensing studies at plot and stand level. Remote Sens. 12, 1–21. https://doi.org/10.3390/rs12030505.

Persson, H.J., Olsson, H., Soja, M.J., Ulander, L.M.H., Fransson, J.E.S., 2017. Experiences from large-scale forest mapping of Sweden using TanDEM-X data. Remote Sens. 9, 1253–1279. https://doi.org/10.3390/rs9121253.

Persson, H.J., Soja, M.J., Fransson, J.E.S., Ulander, L.M.H., 2020. National forest biomass mapping using the two-level model. IEEE J. Sel. Top. Appl. Earth Obs. Remote Sens. 13, 6391–6400. https://doi.org/10.1109/jstars.2020.3030591.

Persson, H.J., Jonzén, J., Nilsson, M., 2021. Combining TanDEM-X and Sentinel-2 for large-scale species-wise prediction of forest biomass and volume. Int. J. Appl. Earth Obs. Geoinf. 96, 10. https://doi.org/10.1016/j.jag.2020.102275.

Piedallu, C., Gégout, J., 2005. Effects of forest environment and survey protocol on GPS accuracy. Photogramm. Remote Sens. 71, 1071–1078.

Ploton, P., Mortier, F., Réjou-méchain, M., Barbier, N., Picard, N., Rossi, V., Dormann, C., Cornu, G., Viennois, G., Bayol, N., Lyapustin, A., Gourlet-fleury, S., Pélissier, R., 2020. Spatial validation reveals poor predictive performance of large-scale ecological mapping models. Nat. Commun. 11, 1–11. https://doi.org/10.1038/s41467-020-18321-y.

Repola, J., 2009. Biomass equations for Scots pine and Norway spruce in Finland. Silva Fenn. 43, 625–647. https://doi.org/10.14214/sf.184.

Rodríguez-Veiga, P., Quegan, S., Carreiras, J., Persson, H.J., Fransson, J.E.S., Hoscilo, A., Ziółkowski, D., Stereńczak, K., Lohberger, S., Stängel, M., Berninger, A., Siegert, F., Avitabile, V., Herold, M., Mermoz, S., Bouvet, A., Le Toan, T., Carvalhais, N., Santoro, M., Cartus, O., Rauste, Y., Mathieu, R., Asner, G.P., Thiel, C., Pathe, C., Schmullius, C., Seifert, F.M., Tansey, K., Balzter, H., 2019. Forest biomass retrieval approaches from earth observation in different biomes. Int. J. Appl. Earth Obs. Geoinf. 77, 53–68. https://doi.org/10.1016/j.jag.2018.12.008.

Saarela, S., Schnell, S., Tuominen, S., Balázs, A., Hyyppä, J., Grafström, A., Ståhl, G., 2016. Effects of positional errors in model-assisted and model-based estimation of growing stock volume. Remote Sens. Environ. 172, 101–108. https://doi.org/10.1016/j.rse.2015.11.002.

Sigrist, P., Coppin, P., Hermy, M., 1999. Impact of forest canopy on quality and accuracy of GPS measurements. Int. J. Remote Sens. 20, 3595–3610. https://doi.org/10.1080/014311699211228.

Smith, R.J., 1993. Logarithmic transformation bias in allometry. Am. J. Phys. Anthropol. 90, 215–228. https://doi.org/10.1002/ajpa.1330900208.

Ståhl, G., Holm, S., Gregoire, T.G., Gobakken, T., Næsset, E., Nelson, R., 2011. Model-based inference for biomass estimation in a LiDAR sample survey in Hedmark County, Norway. This article is one of a selection of papers from Extending Forest Inventory and Monitoring over Space and Time. Can. J. For. Res. 41, 96–107. https://doi.org/10.1139/X10-161.

Ståhl, G., Saarela, S., Schnell, S., Holm, S., Breidenbach, J., Healey, S.P., Patterson, P.L., Magnussen, S., Næsset, E., McRoberts, R.E., Gregoire, T.G., 2016. Use of models in large-area forest surveys: comparing model-assisted, model-based and hybrid estimation. For. Ecosyst. 3, 5. https://doi.org/10.1186/s40663-016-0064-9.

Stehman, S.V., 2009. Model-assisted estimation as a unifying framework for estimating the area of land cover and land-cover change from remote sensing. Remote Sens. Environ. 113, 2455–2462. https://doi.org/10.1016/j.rse.2009.07.006.

Stone, M., 1974. Cross-validatory choice and assessment of statistical predictions. J. R. Stat. Soc. 36, 111–147.

Suty, N., Nyström, K., Ståhl, G., 2013. Assessment of bias due to random measurement errors in stem volume growth estimation by the Swedish National Forest Inventory. Scand. J. For. Res. 28, 174–183. https://doi.org/10.1080/02827581.2012.734329.

Tian, Y., Nearing, G.S., Peters-Lidard, C.D., Harrison, K.W., Tang, L., 2016. Performance metrics, error modeling, and uncertainty quantification. Mon. Weather Rev. 144, 607–613. https://doi.org/10.1175/MWR-D-15-0087.1.

Tomppo, E., Olsson, H., Ståhl, G., Nilsson, M., Hagner, O., Katila, M., 2008. Combining national forest inventory field plots and remote sensing data for forest databases. Remote Sens. Environ. 112, 1982–1999. https://doi.org/10.1016/j.rse.2007.03.032.

Valbuena, R., Mauro, F., Rodriguez-Solano, R., Manzanera, J.A., 2010. Accuracy and precision of GPS receivers under forest canopies in a mountainous environment. Span. J. Agric. Res. 8, 1047–1057. https://doi.org/10.5424/sjar/2010084-1242.

Varvia, P., 2018. Uncertainty Quantification in Remote Sensing of Forests. University of Eastern Finland.

Weber, K.T., 2006. Challenges of integrating geospatial technologies into rangeland research and management. Rangel. Ecol. Manag. 59, 38–43. https://doi.org/10.2111/05-010R.1.

Weber, K.T., Théau, J., Serr, K., 2008. Effect of coregistration error on patchy target detection using high-resolution imagery. Remote Sens. Environ. 112, 845–850. https://doi.org/10.1016/j.rse.2007.06.016.

Wharton, E.H., Cunia, T., 1987. Estimating tree biomass regressions and their error, proceedings of the workshop on tree biomass regression functions and their contribution to the error. Gen. Tech. Reports GTR-NE-117, 303.

Wilks, D., 2011. Statistical Methods in the Atmospheric Sciences, 3rd ed. Academic Press.

Yoshimura, T., Hasegawa, H., 2003. Comparing the precision and accuracy of GPS positioning in forested areas. J. For. Res. 8, 147–152. https://doi.org/10.1007/s10310-002-0020-0.